

INTERNATIONAL ATOMIC ENERGY AGENCY  
UNITED NATIONS EDUCATIONAL, SCIENTIFIC AND CULTURAL ORGANIZATION



INTERNATIONAL CENTRE FOR THEORETICAL PHYSICS  
34100 TRIESTE (ITALY) · P.O.B. 500 · MIRAMARE · STRADA COSTIERA 11 · TELEPHONE: 2340-1  
CABLE: CENTRATOM · TELEX 460892-1

SMR/208 - 4

SPRING COLLEGE IN MATERIALS SCIENCE

ON

"METALLIC MATERIALS"

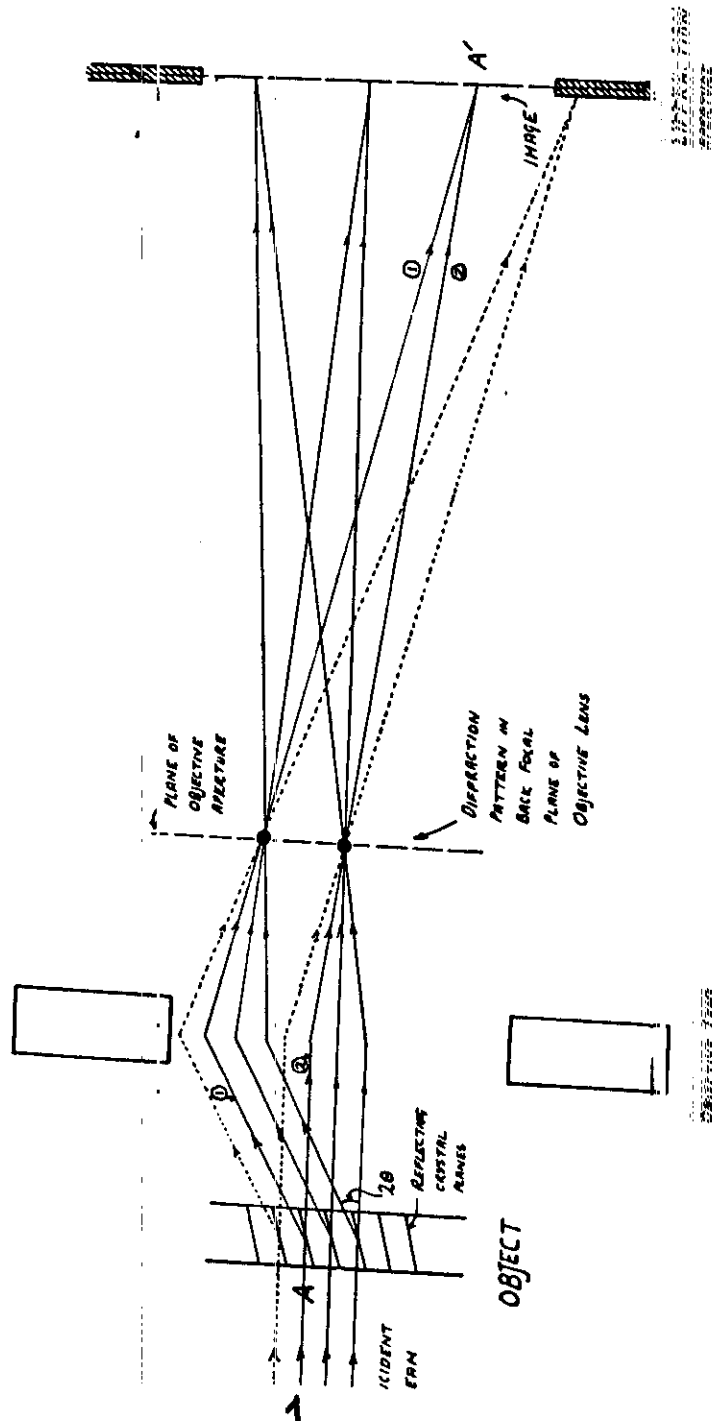
(11 May - 19 June 1987)

TECHNIQUES OF ELECTRON MICROSCOPY

M.L. JENKINS  
Department of Metallurgy  
and Science of Materials  
University of Oxford  
Parks Road  
Oxford OX1 3PH  
U.K.

These are preliminary lecture notes, intended only for distribution to participants.

# PRINCIPLES OF IMAGE FORMATION IN THE ELECTRON MICROSCOPE



2.1.1

## Contrast in the TEM and dark-field techniques

M L Jenkins

Please note that this lecture is meant only to provide a rudimentary guide to contrast mechanisms and microscope techniques so that you can better understand the practical work.

### Suggested reading:

Hirsch, Howie, Nicholson

Pashley and Whelan

Edington

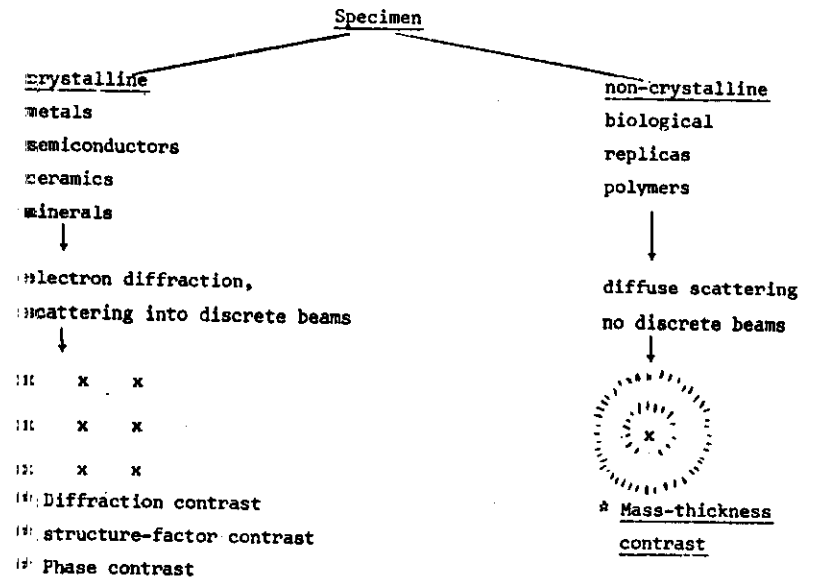
Thomas and Goringe

'Electron microscopy of thin crystals' (1965)  
(available by ordering through Dr M J Whelan)  
'Monographs on practical electron microscopy  
in materials science (4 vols) (1974)  
'Transmission electron microscopy  
of materials' (1979)

### Contrast in the TEM

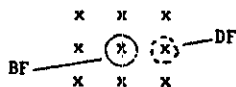
The justification for discussing contrast lies in the necessity to recognize what is seen on the electron-microscope screen and in knowing which experiments to carry out if the image is not immediately recognizable.

There are various contrast mechanisms, applicable to different sorts of specimens and different sorts of problems.



### \* Diffraction contrast

Contrast is produced by allowing only the transmitted beam or one of the diffracted beams to pass through the objective aperture and so form an image. These are called bright-field and dark-field images respectively.



Mechanism: Local variations in diffracted intensity are imaged (to be discussed in detail).

Comments: Most commonly used contrast mechanism, used widely for studying defects in crystals. It is often important to set well-defined diffraction conditions if the image is to be interpreted reliably. A comprehensive theory exists. Image details typically  $\geq 15\text{\AA}$  (depending on imaging conditions).

### \* Structure-factor contrast

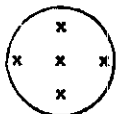
Image formed in same way as in diffraction contrast.

Mechanism: Local variations in structure-factor for the imaging reflection are imaged.

Comments: Examples of this mechanism include in-focus imaging of voids, imaging of amorphous regions in irradiated semiconductors and imaging of disordered zones produced within displacement cascades in ordered alloys.

### \* Phase contrast

Two or more diffracted beams and/or diffuse scattered electrons are recombined to form the image.



Mechanism: Phase changes in the electron waves at the exit surface of the crystal are converted into intensity differences via an additional phase change introduced by the microscope and arising from spherical aberration and defocus.

Comments: This is an important and expanding area of high-resolution applications, including

- \* structure determination and defects in materials such as complex oxides
- \* high-resolution studies of dislocations and interfaces.

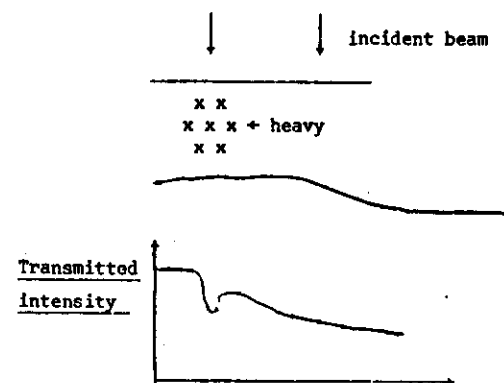
A point-to-point resolution (the first zero of the contrast transfer function near Scherzer defocus) of about  $2.5\text{\AA}$  is available with modern commercial instruments, and special high-voltage high-resolution microscopes approach  $2\text{\AA}$  or better.

$$d_o = 0.70\lambda^{1/2}$$

Detail may be visible in images down to separations  $< 2\text{\AA}$  but may not be interpretable. Comparison of experimental images with computed images is often essential and always desirable.

### \* Mass-thickness contrast

Objective aperture is placed about forward-scattered beam, excluding many of the scattered electrons.



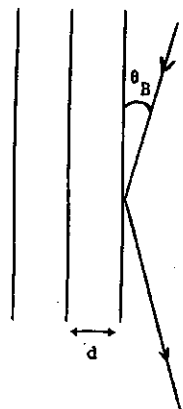
Sometimes called absorption contrast, although the electrons are not really absorbed, they are scattered out of the objective aperture.

Mechanism: Parts of the specimen which are thicker or are composed of elements of higher atomic number will deplete transmitted beam and consequently appear darker.

Comments: Biological specimens are often stained to increase contrast.

# The mechanism of diffraction contrast

Many diffraction contrast effects can be understood without detailed mathematics, bearing in mind only the relatively simple idea of Bragg reflection.



$$2d \sin \theta_B = n\lambda$$

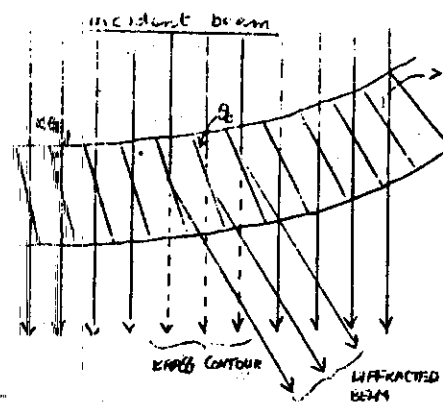
$$\lambda = \frac{h}{p} = 0.037 \text{ \AA} \text{ at } 100 \text{ keV}$$

Examples of effects which can be understood very simply on this basis include bend contours and the contrast of dislocations and precipitates, and these are illustrated on a separate sheet.

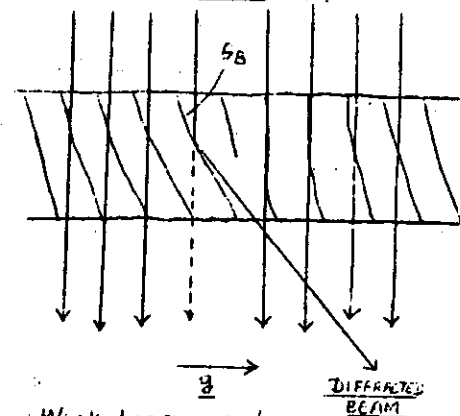
In each case diffraction contrast arises from perturbation of the local diffracting conditions by the defect.

## Diffraction contrast in H<sub>2</sub> TEM

### 1. Bend contours



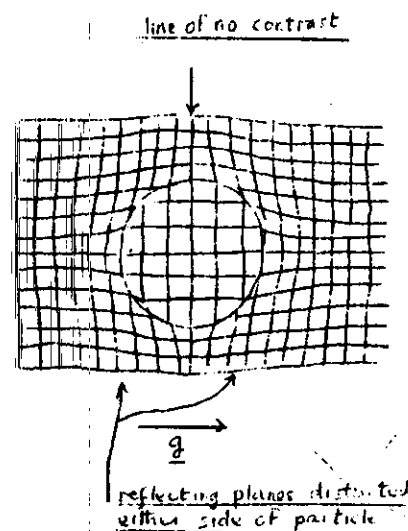
### 2. Dislocation



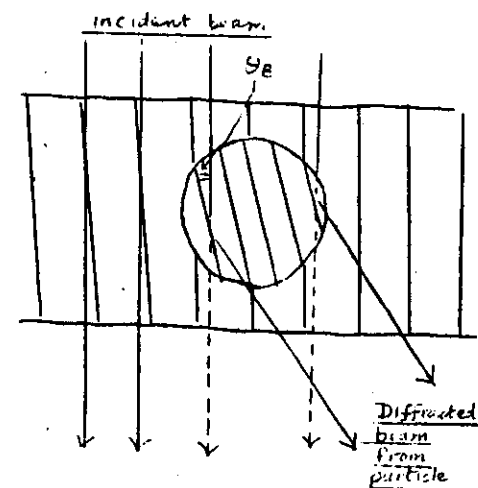
Weak-beam - only near the dislocation core are the planes bent back into the Bragg condition.

### 3. Precipitates

(a) Coherent, with lattice mismatch



(b) Incoherent

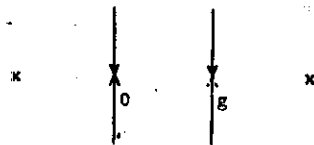


### Setting the diffracting conditions

If images e.g. of dislocations are to be interpreted reliably it is important that well-defined diffracting conditions are set.

This is achieved by tilting the specimen, usually with reference to the Kikuchi pattern.

A common condition used is the strong two-beam condition, with one reflection strongly excited, i.e. at the Bragg condition ( $S_g = 0$ ,  $W = 0$ ,  $E = 1$  see below).



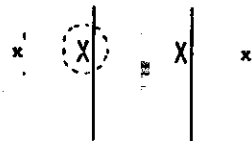
The objective aperture is placed about the forward-scattered beam 0 (bright-field) or the diffracted beam g (dark-field) - often called 'the image in the reflection g'.

Other commonly used conditions include:

### Kinematical (BF)

$$S_g > 0$$

$$E \sim 1.1$$

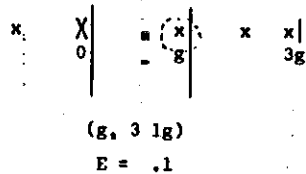


dislocations appear as black-lines (on positive prints)

### Weak-beam (DF)

$$S_g \sim 2 \times 10^{-2} \text{Å}^{-1}$$

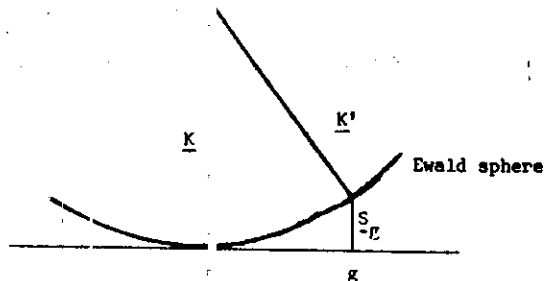
$$W \geq 5$$



dislocations appear as narrow bright lines of high contrast

Deviation parameters used to specify deviation from the Bragg condition.

(i)  $S_g$



$S_g = |S_g|$  and defined as negative (positive) if g lies outside (inside) Ewald sphere.

(ii)  $W = |S_g \xi_g|$  where  $\xi_g$  is the extinction distance. W is dimensionless.

(iii)  $E = [1 + (\frac{S_g}{\xi_g})^2]^{-1/2}$  with  $\theta_g$  the Bragg angle for the reflection g. If  $E = 1, 2, 3$  etc. then the reflections g, 2g, 3g etc. are exactly excited.

### Burgers vector determination

As an example of a typical contrast experiment we consider the determination of the Burgers vector of a dislocation.

The practical procedure is to image the dislocation under two-beam diffraction conditions using various diffraction vectors g in turn. Characteristic invisibility or weak contrast is obtained when  $g \cdot b = 0$ . This condition is sometimes termed the invisibility criterion.

The occurrence of very weak or zero contrast when  $g \cdot b = 0$  can be understood by the following argument:

\* The displacements produced by a dislocation are (mostly) parallel to the Burgers vector b. (For a screw dislocation in an isotropic medium this statement is exact: for an edge dislocation there are also small terms parallel to  $b \times u$ , where u is a unit vector in the direction of the dislocation line).

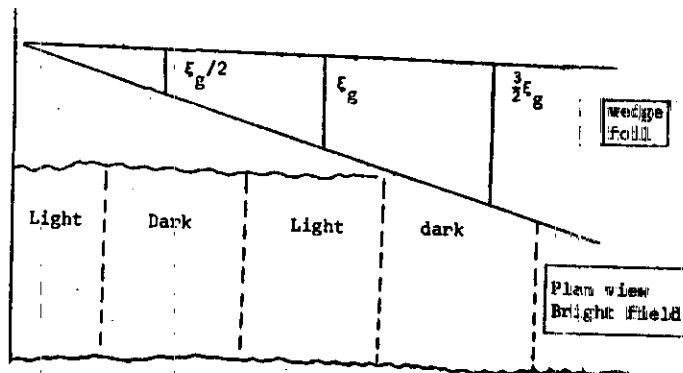
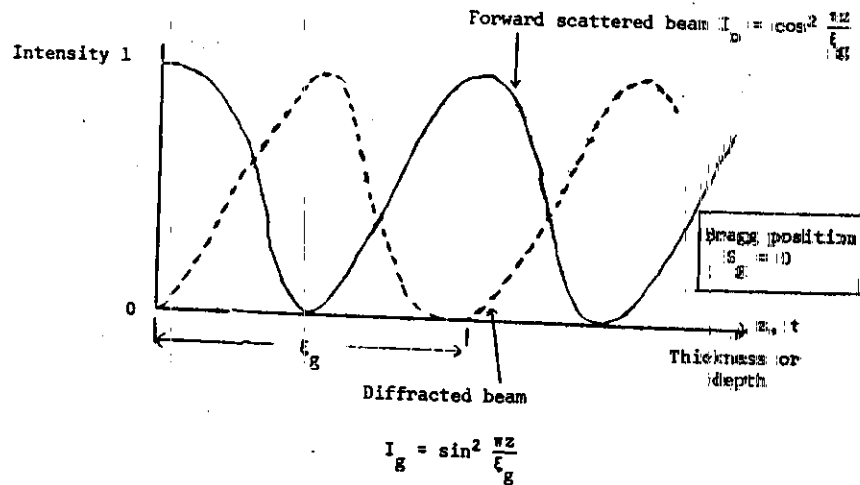
\* The diffraction vector g (reciprocal lattice vector) is perpendicular to the reflecting planes.

\* The dislocation is 'seen' if its strain field bends the diffracting planes. The condition  $g \cdot b = 0$  implies that b is perpendicular to g, so that b lies in the reflecting plane. All displacements are therefore parallel to the reflecting planes - i.e. these planes are not bent. Therefore the dislocation is not seen.

\* For dislocations with edge components the condition  $g \cdot b = 0$  may give weak images but not true invisibility. For true invisibility we require also that  $g \cdot b \times u = 0$ .

### Thickness fringes

Thickness fringes arise because electron scattering is dynamic - i.e. the two-beam case intensity scattered into the diffracted beam is subsequently rescattered back into the forward-scattered beam. The formalism in the two-beam theory with no absorption is given in the section on weak-beam which follows, and leads to the following variation of intensity with thickness or depth:



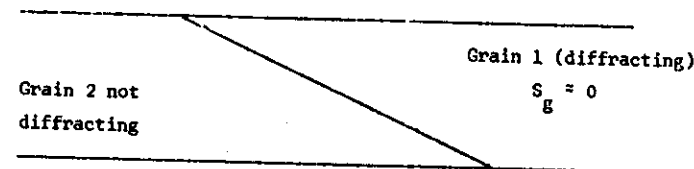
Away from the Bragg condition ( $|S_g| > 0$ ) the coupling between the two beams is less strong, and the depth periodicity is shorter, with effective extinction distance

$$\epsilon_g^{\text{eff}} = \frac{\epsilon_g}{\sqrt{1+w^2}} \quad \text{where } w = |S_g \epsilon_g|$$

The thickness fringes become weaker and crowd closer together

Fringe contrast at planar defects (grain boundaries, stacking faults, antiphase boundaries).

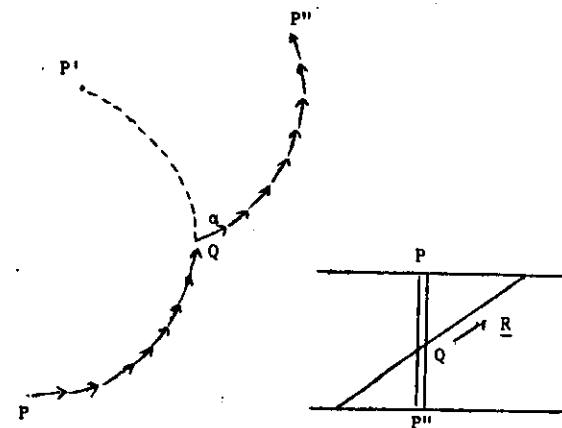
Grain boundary fringes arise in much the same sort of way as thickness fringes, and are particularly easy to understand when one crystal is diffracting strongly and the other is not.



Grain 1 is effectively a wedge-shaped foil, leading to fringes of depth periodicity  $\epsilon_g$ .

The origin of fringes at stacking-faults and similar planar defects is more difficult to understand and requires some knowledge of theory. The contrast arises from a change of phase at the boundary in the scattering contributions to the diffracted beam.

The origin of the contrast is seen qualitatively in the kinematical theory using an amplitude-phase diagram.



Amplitude-phase diagram for a column  $PP''$  containing a fault at  $Q$  with phase angle  $\alpha$ . The resultant amplitude is represented by the vector  $PP''$ ; the amplitude for a corresponding column in a perfect crystal is given by  $PP'$ .

The phase factor  $\alpha$  is given by

$$\alpha = 2\pi \mathbf{g} \cdot \mathbf{R}$$

where  $\mathbf{R}$  is the fault vector. The fault is invisible if  $\alpha = 0$  or is a multiple of  $2\pi$ .

Consider as a specific example a (111) foil of an fcc crystal containing a stacking-fault on the inclined plane (11 $\bar{1}$ ) with fault vector  $\mathbf{R} = \frac{1}{3}[11\bar{1}]$ . Consider imaging the fault in the (2 $\bar{2}$ 0) reflections lying in the (111) reciprocal lattice plane.

$\mathbf{g}$	$\pm 2\bar{2}0$	$\pm 20\bar{2}, 02\bar{2}$
$\alpha$	0	$\pm \frac{8\pi}{3} (= \frac{2\pi}{3})$
	↑ fault invisible	↑ fault visible

In practice the depth periodicity of stacking-fault fringes corresponds roughly at the Bragg condition ( $w = 0$ ) to the extinction distance  $\xi_g$ , and away from the Bragg condition ( $w > 0$ ) to  $\xi_g^{\text{eff}} = \sqrt{1+w^2}$ . The detailed behaviour is quite complicated. Calculations show that in the absence of anomalous absorption the depth periodicity of stacking-fault fringes at the Bragg condition ( $w = 0$ ) would be  $\xi_g/2$ . If we deviate away from  $w = 0$ , alternate fringes become strong and weak, until eventually the weaker fringes disappear and the stronger fringes correspond to a depth periodicity of  $\xi_g^{\text{eff}}$ . In the absence of anomalous absorption, bright-field and dark-field images are complementary. In practical cases the effect of anomalous absorption is to reduce the visibility of fringes near the centre of the foil, and to destroy the complementary nature of BF and DF images. This latter effect can be taken advantage of to determine the nature (intrinsic or extrinsic) of stacking-faults. In addition, anomalous absorption leads to a fringe separation corresponding roughly to a depth periodicity of  $\xi_g$  and not to  $\xi_g/2$  as is the case for no absorption at  $w = 0$ . This occurs by a gradual suppression of alternate fringes, the suppression being greater near the edge of the foil. Weak subsidiary fringes can sometimes be seen near the middle of the foil in relatively thin foils.

#### Forming dark-field images

Two methods:

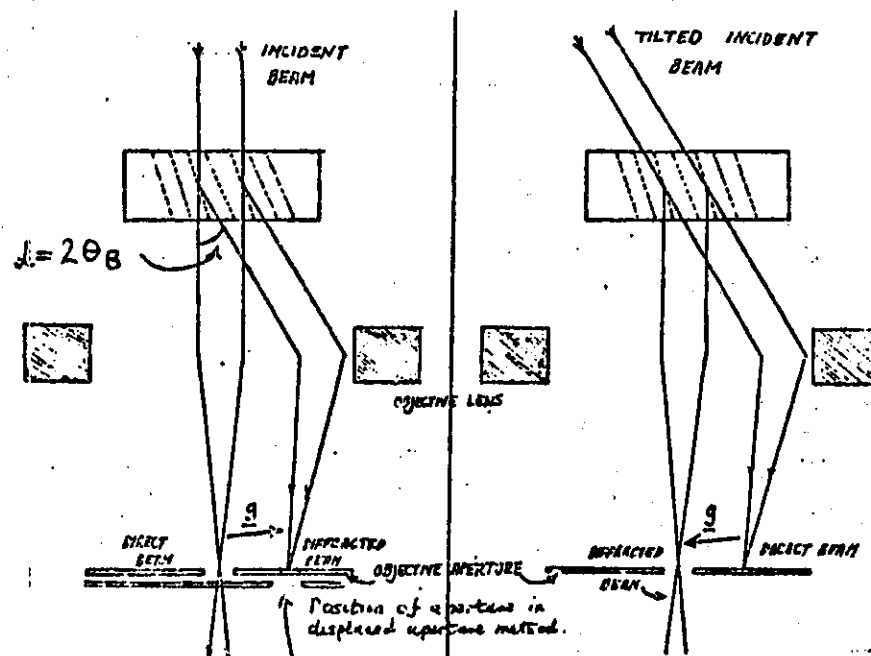
##### 1. Displace the objective aperture

Disadvantage: poor resolution due to 'streaking' parallel to  $\mathbf{g}$  as a result of spherical aberration (see separate sheet).

##### 2. Use beam tilts to bring desired reflection to the optic axis. Almost all microscopes are now equipped with beam-tilting coils.

Disadvantage: tilting the beam alters the diffraction conditions. A 'strong' beam will not remain excited when brought to the centre. In general it will be necessary to reset the desired diffraction conditions by tilting the specimen. One trick to partially get around this problem is to tilt the diametrically opposite diffraction spot to the centre: i.e. if  $\mathbf{g}$  is strongly excited, then tilt  $-\mathbf{g}$  to the axis. When it reaches the axis it will be strongly excited.

## HIGH RESOLUTION DARK FIELD



### Loss of resolution in displaced aperture dark-field images

Spherical aberration has the effect of elongating image points along the direction of  $\mathbf{g}$

The displacement  $R$  of an image formed by a beam making an angle  $d$  with the optic axis (referred to object space) is:

$$R = C_s d^3 \quad \text{--- (1)}$$

In practice the beam always has a finite divergence  $\Delta d$ , leading to a 'smearing' (loss in resolution)  $\Delta R$

$$\Delta R = 3 C_s d^2 \Delta d \quad \text{from (1)}$$

We have  $d = 2\theta_B \approx \frac{\lambda}{d}$  (small angles)

Typical values:  $3C_s = 10^8 \text{ \AA}$ ;  $\Delta d \approx 10^{-3}$  (may be even larger)  
 $\lambda = 0.04 \text{ \AA}$

Giving  $\Delta R = 40 \text{ \AA}$  for  $d = 2 \text{ \AA}$

Note that  $\Delta R \sim \frac{1}{d^2} \rightarrow$  loss of resolution more serious for higher order reflections

### Uses and advantages of dark-field images

1. Simplifying and improving image contrast:
  - \* operating reflection clearly defined
  - \* higher contrast (especially in weak-beam images)
  - \* allows comparisons of experimental and computed images.
2. Obtaining additional contrast information:
  - \* e.g. determining the nature of stacking-faults.
3. Aiding the interpretation of diffraction patterns
  - \* identifying the origin of extra or satellite spots arising from multi-phase specimens, incoherent precipitates etc.
4. Special techniques:
  - \* weak-beam imaging
  - \* structure-factor contrast in ordered alloys.

## 1 Principles of the weak-beam technique

### 1.1. Introduction

Electron microscope images of dislocations taken using strongly excited reflections have image widths  $\sim \xi_g/3$  where  $\xi_g$  is the extinction distance of the operating reflection. On the other hand the dislocation core is only  $\sim 3b$  wide where  $b$  is the magnitude of the Burgers vector. Consequently the normal 'image' of a dislocation shows contrast for very small disturbances of the crystal. This wide image has come to be an accepted property of dislocations, and its disadvantages are often overlooked. For example in a great many investigations the accurate position of the dislocation core (or cores) is sought. From images  $\sim \xi_g/3$  wide such determinations are difficult especially when the dislocation geometry is complicated (e.g. dissociated), and often complex computer simulation techniques must be employed. The weak-beam method simply replaces these wide images with narrow ( $\sim 15\text{\AA}$ ) intense ( $\sim 100$  times background) image peaks close to, and at a determinable distance ( $\sim 20\text{\AA}$ ) from the dislocation cores. Each dislocation core shows an intensity peak on a uniform background, and consequently the geometry and interactions of strain fields can be accurately determined.

### 1.2. Theory

For simplicity we consider the scattering equations in the two beam form without absorption. (Extension to a more general analysis is straightforward). In a perfect crystal the relationship between the amplitudes  $\phi_g$  of the diffracted beam and  $\phi_0$  of the forward scattered beam is

$$\frac{d\phi_0}{dz} = -\frac{\pi i \phi_g}{\xi_g}$$

$$\frac{d\phi_g}{dz} = \frac{\pi i}{\xi_g} \phi_0 + 2\pi i s \phi_g \quad (1)$$

where  $z$  is the depth in the foil,  $\xi_g$  is the extinction distance, and  $s (= w/\xi_g)$  is the distance of the Ewald sphere from the reciprocal lattice point  $g$ . When  $s = 0$ , the crystal is in the Bragg orientation, and the strong coupling between  $\phi_0$  and  $\phi_g$  produces the Pendellösung oscillation with depth shown in fig.1a. When  $|s|$  is large, the crystal is far from the Bragg orientation and the weak coupling between  $\phi_0$  and  $\phi_g$  results in the kinematical oscillation with depth shown in fig.1b.



For an imperfect crystal, equation 1 is replaced by

$$\frac{d\phi_0}{dz} = \frac{\pi i \phi_g}{\xi_g}$$

$$\frac{d\phi_0}{dz} = \frac{\pi i}{\xi_g} \phi_0 + 2\pi i (s_{\text{eff}}) \phi_g \quad (2)$$

$$\text{where } s_{\text{eff}} = s + g \cdot \frac{dR(z)}{dz}$$

with  $R(z)$  being the local displacement of the crystal from its perfect crystal position. By analogy with eqn 1, eqn 2 describes strong coupling between  $\phi_0$  and  $\phi_g$  if  $s_{\text{eff}} = 0$ , i.e. if  $s + g \cdot \frac{dR(z)}{dz} = 0$ . This is the condition that the local displacement  $R(z)$  orients or 'twists' the crystal planes into the Bragg condition.

Let us now consider the crystal model shown in fig. 2a. In regions AB and CD the crystal is far from the Bragg condition but in region BC it is at the Bragg condition. In region AB the weak coupling between the incident and diffracted beams means that the diffracted beam has only a kinematic oscillation with depth (fig. 2b) and little energy is transferred. In region BC the strong coupling transfers energy as in the initial stages of the Pendellosung curve of fig. 1a. In region CD there is again only weak coupling, and the kinematic oscillation returns. However the increased energy in the diffracted beam (fig. 2b) is retained and not lost. For the case when there are more than two beams to be considered the system is slightly more complicated (fig. 2c) but the increased intensity in the weak-beam is still obtained.

### 1.3. Undissociated dislocations

Consider an edge dislocation with line and Burgers vector parallel to the plane of the foil (fig. 3). We expect a weak-beam peak to occur for the column PP' in which the lattice planes are at the Bragg condition at a turning point of  $\frac{dR(z)}{dz}$ . For columns to the left of PP', the lattice planes never attain the Bragg condition while for columns to the right the Bragg condition is passed through rapidly as a function of depth. On the other side of the core, the lattice bending is in the opposite direction. Therefore we expect a weak-beam peak to occur for any column in which  $g \cdot \frac{dR(z)}{dz} = -s$  at a turning point of  $g \cdot \frac{dR(z)}{dz}$ . Similar conclusions (with minor alterations) can be obtained from the Bloch-wave formulation.

In order to check the predictions given above, many-beam calculations were performed for an undissociated edge dislocation lying in the plane of a (111) foil of copper, with  $b = \frac{a}{2}[\bar{1}10]$  and assuming a strain field based on isotropic elastic continuum theory. The weak-beam image for the reflection  $g = 2\bar{2}0$  was investigated for the dislocation at various depths in foils of various thickness. Six systematic reflections were included in the calculation, and the absorption parameters of Humphreys and Hirsch (1968) were used with 100keV electrons. In all cases, a single, narrow ( $\sim 15\text{\AA}$  at half height), intense ( $\sim 100$  times background) peak was observed, and its position was given to  $\pm 7\text{\AA}$  by the condition discussed above viz  $g \cdot \frac{dR(z)}{dz} = -s$  at a turning point of  $g \cdot \frac{dR(z)}{dz}$ . For certain geometries the peak intensity can be greatly reduced, although in general it is much greater than background.

### 1.4. Dissociated dislocations

Consider the dislocation discussed above dissociated according to the equation  $b = \frac{a}{2}[\bar{1}10] + \frac{a}{6}[\bar{1}2\bar{1}] + \frac{a}{6}[\bar{2}11] = b_1^P + b_2^P$ . For  $g = 2\bar{2}0$  there is no stacking fault contrast. Associated with each core there is expected to be a weak-beam peak, one lying outside the two partials and the other between them (as can be confirmed by sketching the lattice plane configurations). Their positions predicted by the criterion given above for the dislocation in edge orientation are

$$x = (2 + CA \pm \sqrt{4 + C^2 A^2}) / 2C$$

$$\text{where } C = -s / \left( \frac{g \cdot b}{2\pi} \left[ 1 + \frac{1}{2(1-\nu)} \right] \right)$$

with  $\nu$  being Poisson's ratio and the peak separation is  $\Delta_{\text{obs}} = \sqrt{\Delta^2 + 4/C^2}$  where  $\Delta$  is the partial separation. (For the dislocation in other orientations, the expressions are similar.) Many-beam computations confirm the accuracy of these relations to  $\pm 7\text{\AA}$  for various depths of dislocation and thickness of crystal.

It is clear that the method provides an accurate means for determining small separations of partial dislocations, and has now been applied to many systems.

### 1.5. Restrictions

It is clear that the advantage of weak-beam images over normal strong-beam images is that weak-beam images show a very uniform background except for a very narrow intensity peak defining the dislocation position. To obtain these conditions, computed images indicate that  $|s|$  must be  $> 2.0 \times 10^{-2} \text{\AA}^{-1}$  for 100keV electrons. It has been found easiest to obtain this condition by setting up a line of systematic reflections, from which the geometry can easily be determined.

However such an arrangement is not necessary. All that is required is that, for the reflection in question,  $|s|$  should be sufficiently large. In copper, this corresponds to nearly satisfying the  $6\bar{6}0$  reflection for a  $2\bar{2}0$  weak-beam image. As a result, very weak images, normally not observable on the screen, are obtained.

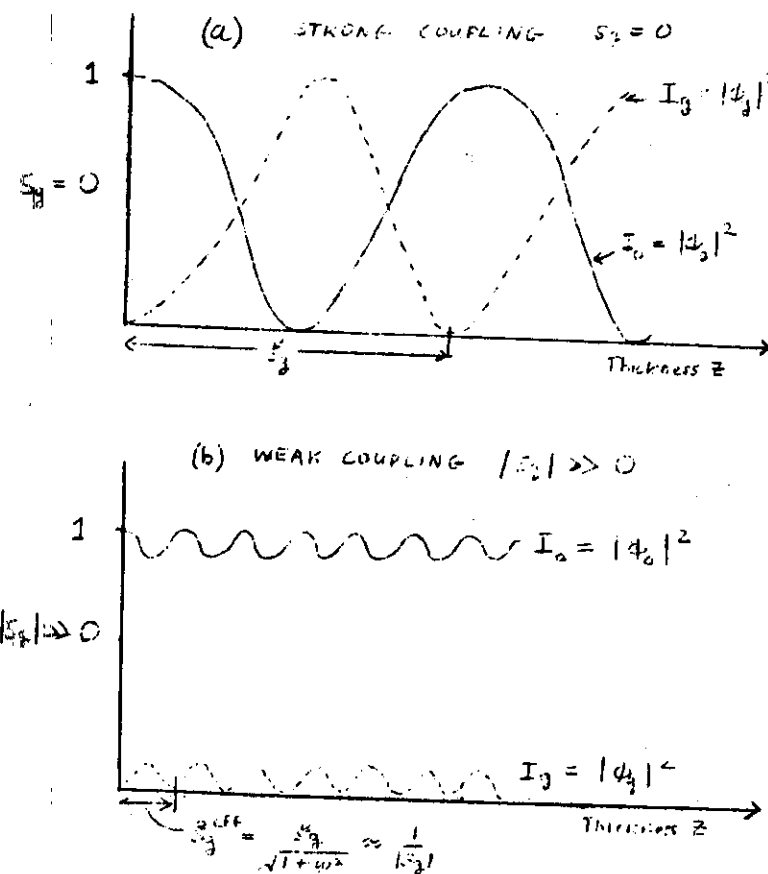


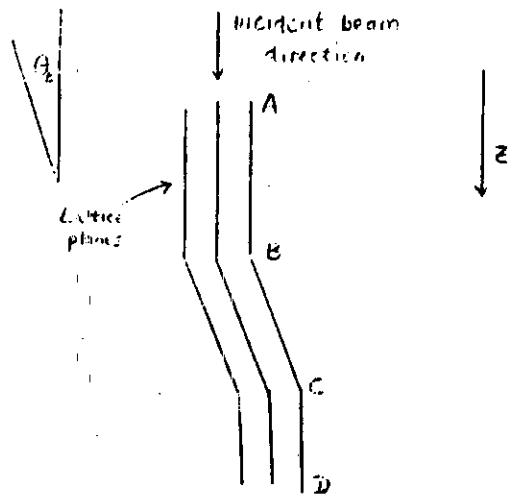
FIGURE 1 Depth dependence of scattered intensities as a function of  $S_g$

$$I_g = \sin^2 \beta \sin^2 \left( \frac{\pi z}{S_g \sin \beta} \right)$$

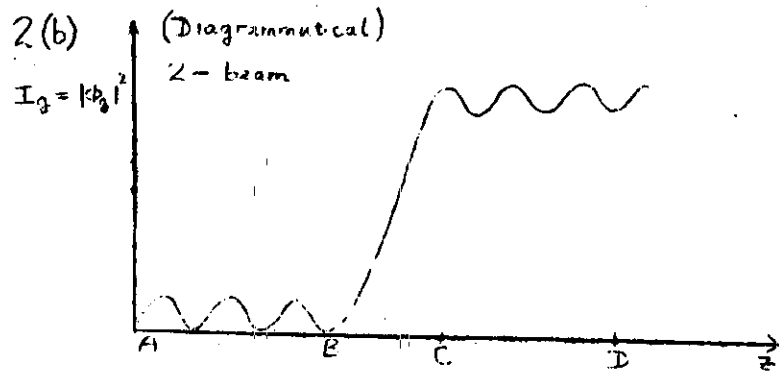
$$\text{at } \beta = \omega = S_g S_g$$

$$I_0 = 1 - I_g$$

2(a)



2(b)



2(c)

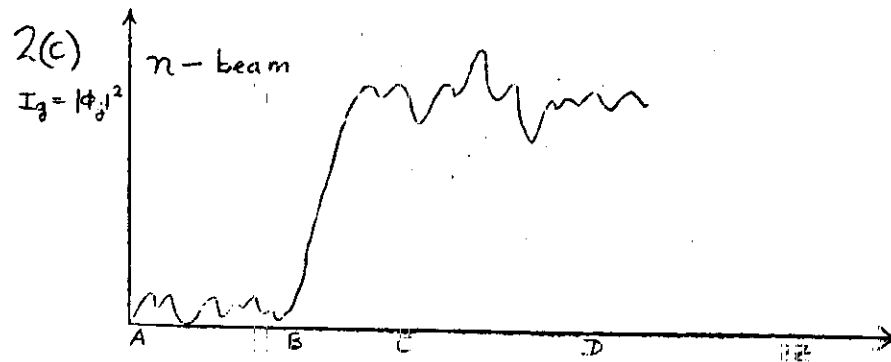
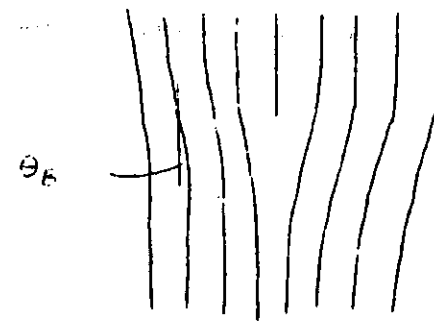


FIGURE 2

Beam



Distance from slip plane (A)

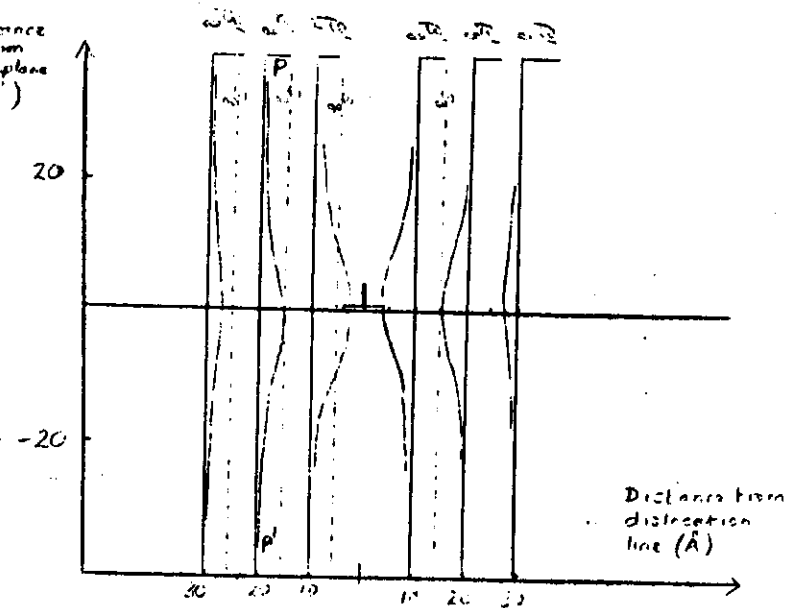
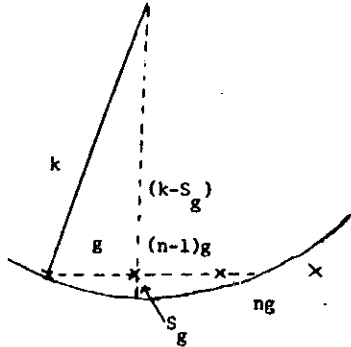


Figure 3 The value of  $\beta'_g = \frac{1}{2} \cdot \frac{dR}{dz}$  down columns at various distances from an edge dislocation lying parallel to the foil. The weak-beam peak is expected to occur for the column in which  $-S_g = \beta'_g$  at a turning point of  $\beta'_g$  (is column PP')

To determine  $|S_g|$  from the diffraction pattern

\* The most common way to obtain weak-beam images is to image in the reflection  $g$  with the 'reflection'  $ng$  excited.  $n$  need not be integral, and in general one should avoid exactly exciting any other reflections whether systematic or non-systematic.



$$k = \frac{1}{\lambda}$$

$$g = \frac{1}{d}$$

$ng$  is satisfied.  
 $S_g$  refers to  $g$  and is positive if  $g$  lies inside sphere, as shown.

For chords of a circle intersecting at right angles:

$$(2k - S_g) S_g = (n-1) g^2$$

To first order in  $S_g$ :

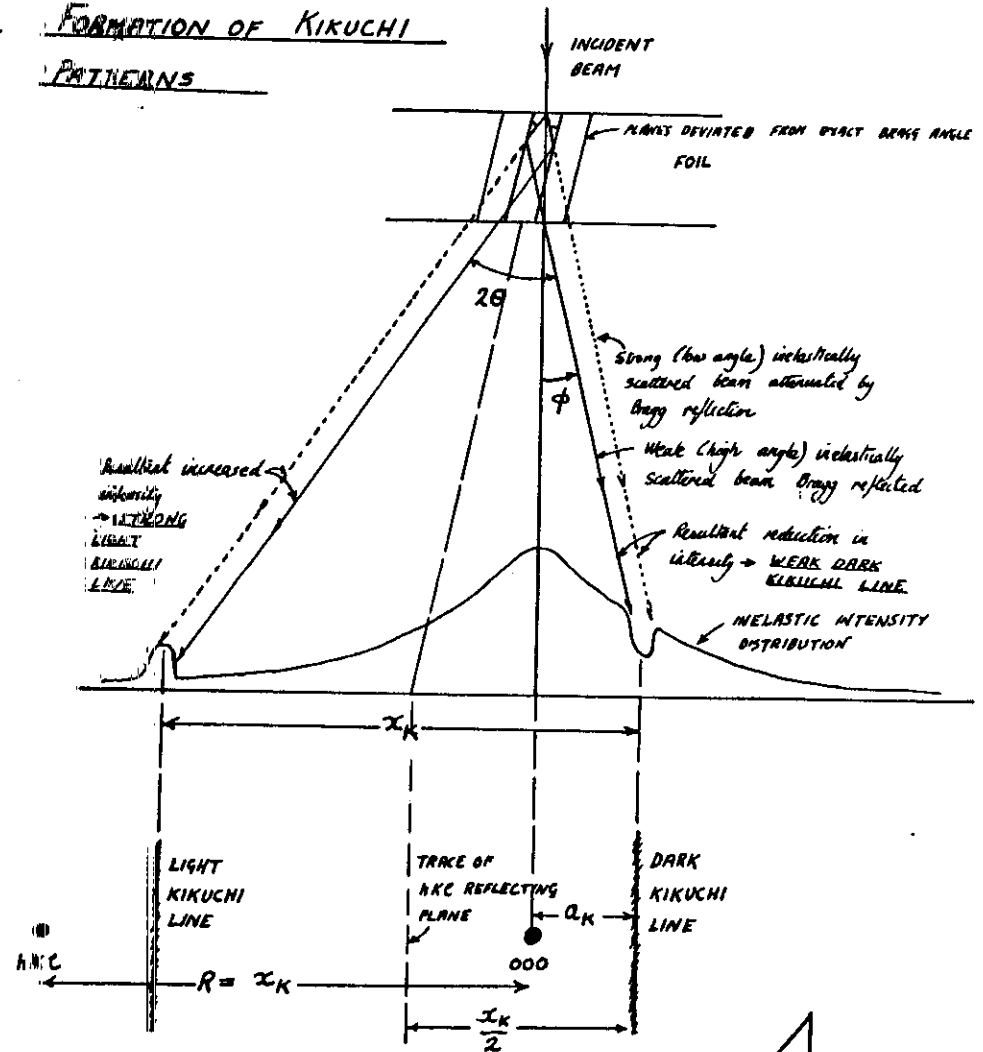
$$S_g = \frac{(n-1) g^2}{2k}$$

\* A less common way to obtain weak-beam images is to image in the reflection  $-g$  with the reflection  $ng$  excited. A similar argument gives the deviation parameter in this case as:

$$S_{-g} = - \frac{(n+1) g^2}{2k}$$

The sign is negative because  $-g$  lies outside the Ewald sphere.

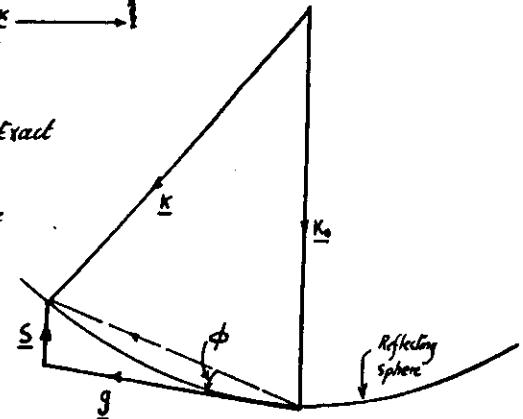
## FORMATION OF KIKUCHI PATTERNS



$\phi$  = Deviation of reflecting planes from Exact Bragg position

$$\phi = a_K / L \quad (\text{When } a_K = 0, \phi = 0, \text{ i.e. exact Bragg condition})$$

$||S|| = \phi |g|$  = Distance of RELP from Reflecting Sphere



### Lattice Imaging

Under optimum conditions high resolution lattice imaging provides a projection of the molecular structure of a suitably oriented crystal or other specimen. Resolution of useful 2-D structure images will be at 1.5 - 5Å and 1-D lattice images 0.5 - 100Å, depending primarily on the microscope, the structure and the problem. From such images of very thin crystals or amorphous material, it is possible directly to interpret features of both unknown but periodic unit cell structures and of the aperiodic modification introduced by defects, e.g. dislocations, precipitates, boundaries, loss of crystallinity, radiation damage etc. However, at the atomic level the scattering and image forming processes are relatively complex so that it is usually necessary, and always wise, to confirm an intuitive or 'by inspection' interpretation. This is done by careful control of the experimental conditions, including recording a series of related images and comparing them with those calculated from model structures. This is required because of the influences of local orientation and thickness of the specimen, the potential complexity of the electron scattering processes involved and the influence of the microscope aberrations on the image contrast through the contrast transfer function (CTF). This latter is used to describe and evaluate the usefulness of microscopes for high resolution work. Goniometer specimen stages are usually essential.

It will be shown that any reasonably modern microscope can be used for very useful lattice imaging, including to complement other forms of microscopy, but that the requirements for the highest resolution are rather more stringent, sometimes requiring access to more specialised equipment. Current developments in digital on-line image processing and alternative imaging methods will be introduced. Applications illustrated include phase transformation studies in metals, ceramic and catalyst identification, structural studies of semiconductor materials and of some organic materials.

References: Proc. 47th Nobel Symposium, 1979 *Chemica Scripta* 14 (1979).  
J.C. Spence, *Experimental High Resolution Electron Microscopy*  
OUP 1981.

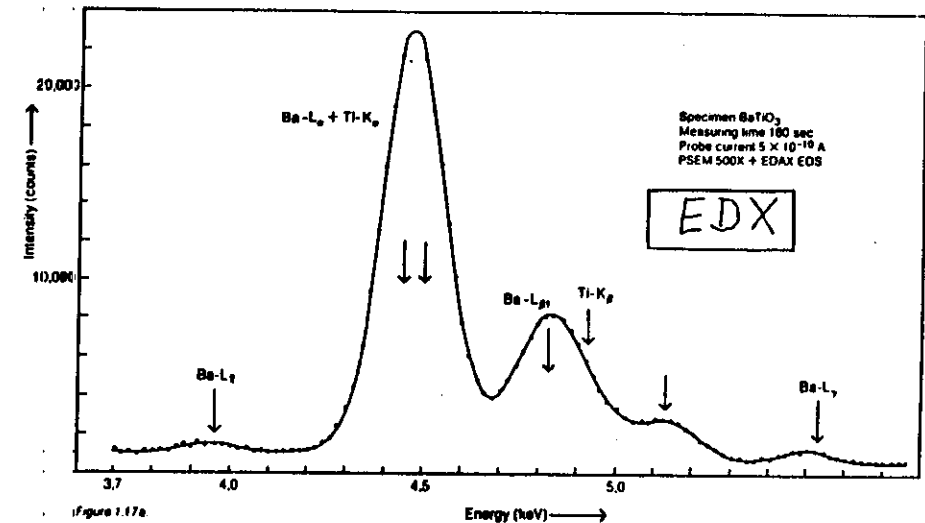


Figure 1.17a

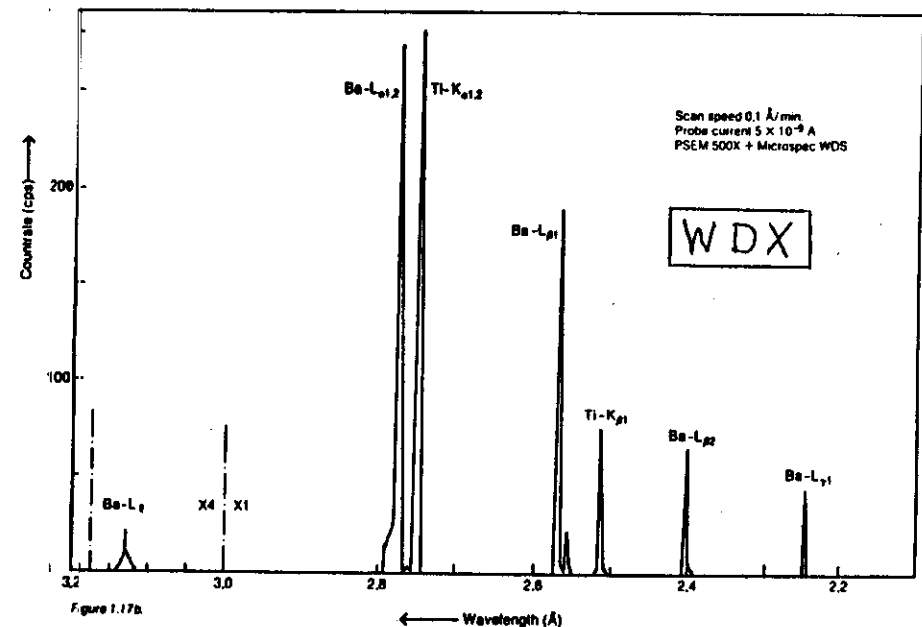


Figure 1.17b

Figure 1.17a, b. X-ray spectra of BaTiO<sub>3</sub>: a) EDS b) WDS.

## X-RAY ANALYSIS IN THE TRANSMISSION ELECTRON MICROSCOPE

### 1. X-ray Production

When electrons of sufficient energy are incident on a specimen X-rays are produced. These X-rays are of two types: 'white' or 'background' radiation produced by the deceleration of the incident electrons and characteristic radiation produced by electronic transitions within individual atoms.

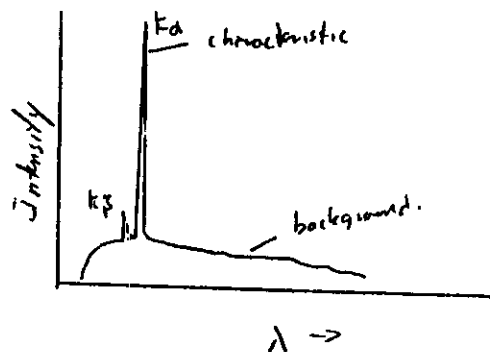


Figure 1. X-ray spectrum showing characteristic and background radiations.

The wavelength (and energy) of the characteristic X-rays varies systematically with the atomic number  $Z$ . Thus if the wavelength or the energy of the X-rays emitted by the sample can be determined, a chemical analysis can be carried out.

### 2. Comparison of Energy Dispersive and Wavelength Dispersive Detectors.

The wavelength  $\lambda$  and energy  $E$  of X-rays (in fact all electromagnetic radiation) are related.

$$E = \frac{hc}{\lambda} \quad \text{or} \quad E(\text{keV}) \approx \frac{12.4}{\lambda(\text{\AA})}$$

where  $h$  = Planck's constant and  $c$  = velocity of light.

Thus either a wavelength dispersive (a crystal spectrometer) or an energy dispersive (solid state) detector can be used to divide an X-ray signal into its elemental components. The characteristics and relative advantages of the crystal spectrometer and the energy dispersive detector are summarised in the following table.

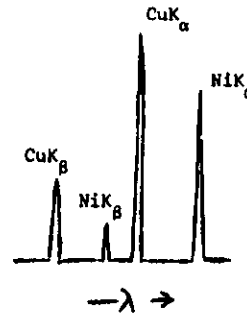
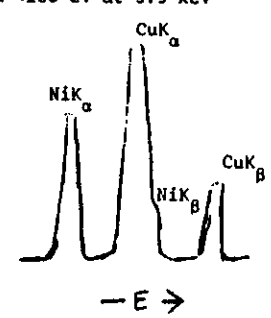
CHARACTERISTICS	WAVELENGTH DISPERSIVE	ENERGY DISPERSIVE
Discrimination	Excellent	FWHM $\sim 150$ eV at 5.9 keV
e.g. Ni, Cu		
Count Rate	30,000 cps (one channel)	2,000-10,000 cps (entire spectrum)
Peak-to-background (thin sample)	200:1	50:1
Light Element Limit	$Z > 4$ (Be)	$Z \geq 11$ (Na)
Solid Angle	0.01	0.05
Number of Elements	1 per spectrometer	all elements $Z \geq 11$ analysed simultaneously
Stability required of source	high	none
Stability of detector	good short term poor long term	excellent
operation	requires a skilled operator	operator proof

Table 1. Comparison of Performance of Energy Dispersive and Wavelength Dispersive X-ray Detectors.

### 2. Analysis of Bulk Specimens

In a bulk specimen the incident electron beam diffuses into a large pear-shaped volume beneath the specimen and X-rays are produced throughout this volume.

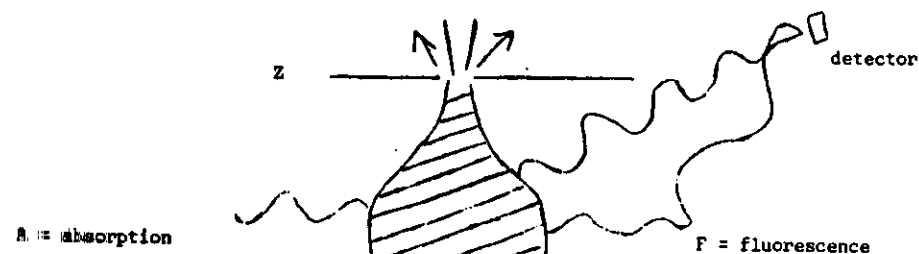


Figure 3. X-ray production in a bulk specimen.

When quantitative analyses are carried out it is necessary to compare the observed X-ray intensities with those from bulk standards and then make corrections for backscattering (Z) absorption (A) and fluorescence (F). As it is necessary to know the composition of the specimen to make the corrections, an iterative procedure is applied, usually using a computer.

#### 4. Analysis of Thin Specimens

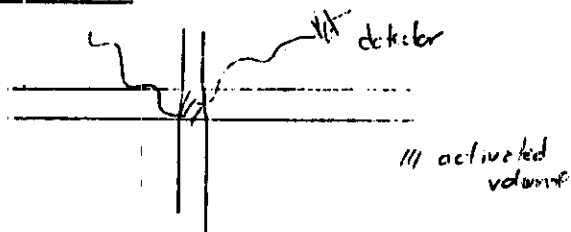


Figure 3. X-ray production in a thin foil

In a thin specimen the large bell-shaped region is absent and the analysis volume is approximately equal to a cylinder of the probe diameter. Thus the spatial resolution for analysis is measured in hundreds or thousands of  $\mu$  rather than in  $\mu$ m as is the case in bulk specimens. The absolute intensity of the characteristic X-rays produced in a thin foil cannot be compared with a bulk standard because it will be function of specimen thickness as well as composition.

If the specimen is sufficiently thin to carry out microscopy at 100 kV then, to a first approximation, X-ray absorption and fluorescence in the specimen can be ignored. Thus while the absolute characteristic X-ray intensity for any one element will be a function of specimen thickness, the characteristic X-ray intensity ratio for any two elements is independent of thickness, i.e.

$$\frac{C_1}{C_2} = k \frac{I_1}{I_2}$$

where  $I_1$  and  $I_2$  are the observed characteristic X-ray intensities,  $C_1$  and  $C_2$  are the weight fraction ratio of the two elements and  $k$  is a factor which must be either calculated or determined experimentally. If the highly stable energy dispersive detector is used in combination with a thin specimen it is possible to calibrate an instrument so that the relevant  $k$ 's can be determined from the specimens of known composition.

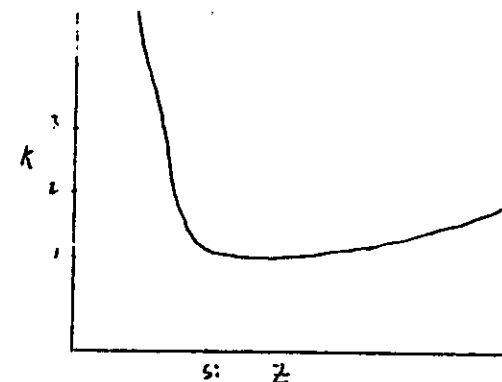


Figure 4. Calibration curve of  $k$  vs  $Z$

A schematic calibration curve is shown in Figure 4. This can be used to convert the observed X-ray intensity ratios into weight fraction ratios.

The shape of the calibration curve can be explained by considering the efficiency of X-ray production as a function of  $Z$  and the preferential absorption of low energy X-rays in the Be window of the detector.

The assumption of no absorption in the specimen will clearly break down for 'thick' samples and low energy X-rays and it is important to know the specimen thickness to check if the 'thin film criterion' holds. During the analysis a contamination spot is formed on both the top and bottom of the foil. If the sample is tilted  $30^\circ$  or  $40^\circ$  after the analysis and the distance between the spots measured the specimen thickness is readily determined. The standard X-ray absorption equation

$$I = I_0 e^{-\frac{\mu}{\rho} \rho x}$$

where  $I$  and  $I_0$  are the transmitted and initial X-ray intensities, respectively,  $(\frac{\mu}{\rho})$  is the mass absorption coefficient,  $\rho$  is the density and  $x$  the sample thickness, is applied to each observed characteristic X-ray intensity and, if necessary, modify the 'thin film' result.

#### 5. The Spatial Resolution for the Analysis of Thin Films.

In a very thin foil the spatial resolution will be given by the probe diameter. The maximum current that can be obtained in a probe of diameter  $d$

is given by

$$i_{\max} = \frac{3\pi^2\beta}{16} \left[ \frac{d^{8/3}}{Cs^{2/3}} - \frac{4}{3} (1.22\lambda)^2 \right]$$

where  $\beta$  is the brightness of the gun,  $C_s$  the spherical aberration coefficient of the probe-forming lens and  $\lambda$  the electron wavelength. In a modern 100 kV transmission electron microscope, which uses the pre-field of the objective as the probe-forming lens,  $C_s = 1.2$  mm and, for a conventional thermionic W emitter,  $\beta = 1 \times 10^5$  amps  $\text{mm}^{-2}$  steradian $^{-1}$ . Under these conditions it is possible to focus a current of  $\sim 10^{-9}$  amps (the minimum for quantitative analysis) into a probe  $\sim 20$  Å in diameter.

A dramatic improvement in performance can be obtained by replacing the W thermionic emitter with a cold field emission tip,  $\beta = 500 \times 10^{15}$  amp  $\text{cm}^{-2}$  steradian $^{-1}$ . However, the stable operation of a field emission tip requires UHV conditions, i.e.  $10^{-9}$ - $10^{-10}$  torr as compared to the  $10^{-5}$  torr of a conventional electron microscope. With a field emission tip and a  $C_s$  value of 1-2 mm a current of  $10^{-10}$  to  $10^{-9}$  amps can be focussed into a probe of diameter  $\sim 10$  Å.

When the incident probe is essentially a point source of electrons it is important to examine the divergence of the electron beam as it passes through the specimen: the activated volume will no longer approximate a cylinder of diameter equal to that of the incident probe.

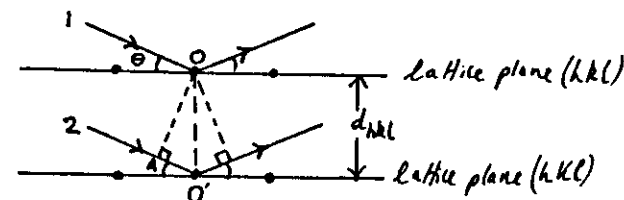
#### References

- Goodhew, P.J., *Electron Microscopy and Analysis*, Wykeham, London, 1975.
- Cliff, G. and Lorimer, G.W., *The Quantitative Analysis of Thin Films*, (1975) J. Microsc. 103, 2-3.
- Lorimer, G.W., Cliff, G. and Clark, J.N., *Determination of the Thickness and Spatial Resolution for the Quantitative Analysis of Thin Films*. In *Developments in Electron Microscopy and Analysis*, Ed. U. Wenzel, Academic, London, 1976, p.153.
- Chandler, J.A., *X-ray Microanalysis in the Electron Microscope*, in *Practical Methods in Electron Microscopy*, Volume 5, Part II, Ed. H.A.N. Clavert, North-Holland, Amsterdam, 1977.

#### Geometry of electron diffraction

##### Bragg's Law

The radiation is considered to be reflected from the lattice planes of the crystal. The path



difference between rays 1 and 2 is  $2 \times AO' = 2 d \sin \theta$ . For reinforcement of the rays the path difference must be a whole number of wavelengths:

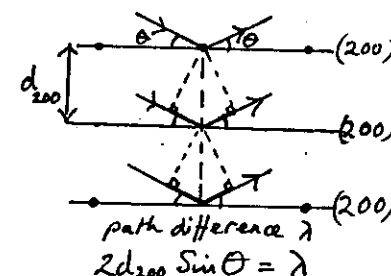
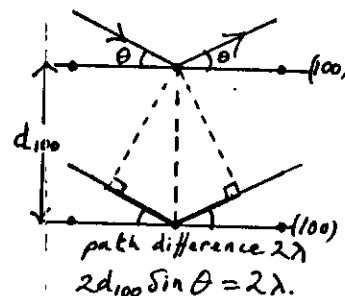
$$2d \sin \theta = n\lambda \quad \lambda - \text{wavelength, } n - \text{integer.}$$

This is Bragg's Law.

It is usually written :

$$2d \sin \theta = \lambda \quad \text{i.e. } n = 1.$$

Rather than referring to the second order reflection from the (100) planes ( $n = 2$ ), we refer to the first order reflection from the (200) planes or simply the 200 reflection.



i.e. the  $n$  is absorbed into the indices.

Note the omission of the brackets from the indices of a reflection; the (hkl) planes give rise to the hkl reflection.

The interplanar spacing  $d_{hkl}$  is related to the unit cell dimensions. For orthogonal crystals (cubic, tetragonal, orthorhombic):

$$\frac{1}{d_{hkl}^2} = \frac{h^2}{a^2} + \frac{k^2}{b^2} + \frac{l^2}{c^2}$$

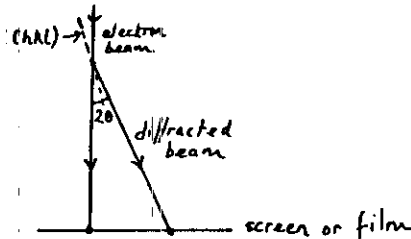


For cubic crystals :

$$d_{hkl} = \frac{a}{\sqrt{h^2 + k^2 + l^2}}$$

### The reciprocal lattice

The angle that the diffracted beam makes with the direct beam is  $2\theta$ . The distance of the



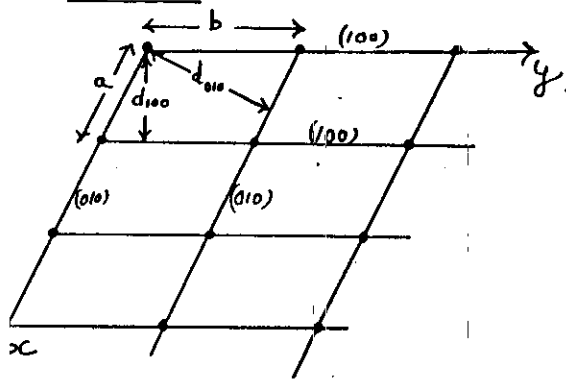
spot from the centre of the diffraction pattern is thus proportional to  $2\theta$ . But from Bragg's law :

$$\sin \theta \sim \theta = \frac{\lambda}{2d} \quad (\theta \text{ small})$$

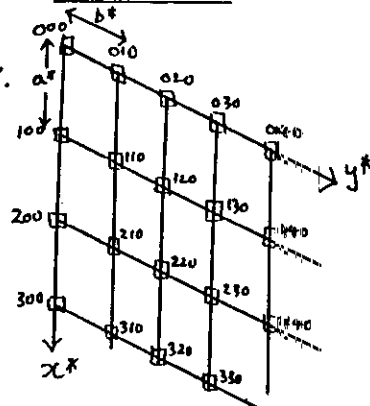
i.e. there is a reciprocal relationship between the direct lattice spacing  $d_{hkl}$  and the distance of the corresponding reflection from centre of the diffraction pattern. The reflections are said to constitute the reciprocal lattice.

A set of planes of spacing  $d$  in the direct lattice produces a reflection in the reciprocal lattice at a distance  $g = 1/d$  from the origin and in the direction of the normal to the planes.

### Direct lattice



### Reciprocal lattice



The axes of the reciprocal lattice are  $x^*$ ,  $y^*$ ,  $z^*$  and have repeats  $a^*$ ,  $b^*$ ,  $c^*$  where :

$$a^* = \frac{1}{d_{100}}, \quad b^* = \frac{1}{d_{010}}, \quad c^* = \frac{1}{d_{001}}$$

The origin of the reciprocal lattice (the direct beam) is 000. These relationships hold for any system.

For orthogonal systems only :

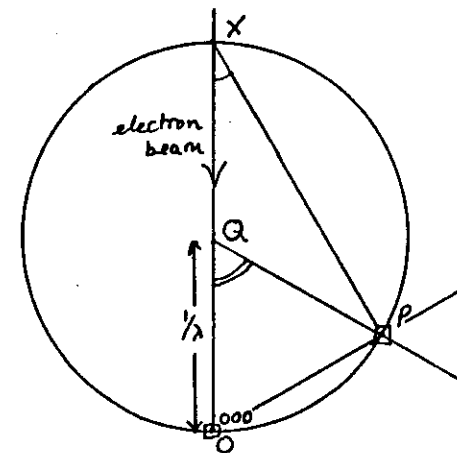
$$a^* = \frac{1}{a}, \quad b^* = \frac{1}{b}, \quad c^* = \frac{1}{c}$$

In general  $\mathbf{g}_{hkl} = \frac{1}{d_{hkl}} = h\mathbf{a}^* + k\mathbf{b}^* + l\mathbf{c}^*$ .

Indices can be added vectorially

$$\text{e.g. } \mathbf{g}_{210} = \mathbf{g}_{200} + \mathbf{g}_{010}$$

### The reflecting sphere



If  $P$  is a reciprocal lattice point  $hkl$  and it lies on a sphere which has the incident beam as a diameter, 000 on the circumference and a radius of  $1/\lambda$ , then  $P$  is correctly oriented for Bragg diffraction because :

$$\mathbf{g} = \frac{\mathbf{OP}}{d} \therefore \mathbf{XP} \text{ is trace of } (hkl). \text{ (normal to } g).$$

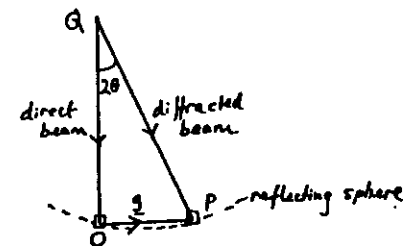
$$\therefore \angle OXP = \theta \text{ and } \angle QP = 2\theta.$$

$$\text{From } \triangle OXP: \sin \theta = \frac{OP}{OX}$$

$$= \left(\frac{1}{d}\right) / \left(\frac{2}{\lambda}\right)$$

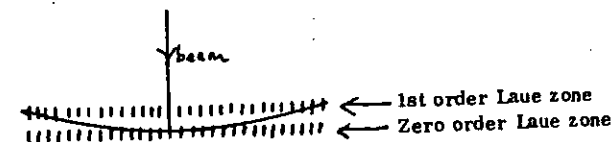
$$\text{or } 2d \sin \theta = \lambda \quad \text{Bragg's Law}$$

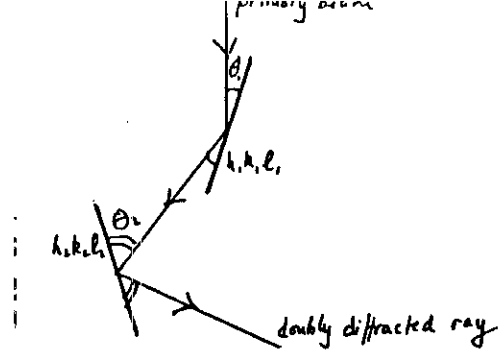
As  $\angle QP = 2\theta$ ,  $QP$  is the direction of the diffracted ray.



Given the seemingly stringent conditions for reflection why do we see a diffraction pattern on the screen? Because :

- reflecting sphere is very large ( $\lambda_{100 \text{ kV}} = 0.037 \text{ \AA}$ )
- 'spots' are streaked out perpendicular to foil because of its finite thickness ( $\leq 0.2 \mu\text{m}$ ).





The reflection appears to have come from a plane (hkl) where :

$$h = h_1 + h_2, \quad k = k_1 + k_2, \quad l = l_1 + l_2.$$

**Reference :**

Crystallography. R. Steadman. van Nostrand Reinhold, 1982.

Electron diffraction in the electron microscope. Practical electron microscopy in materials science Vol. 2. J.W. Edington. Philips Technical Library, 1975.

## X-ray Production

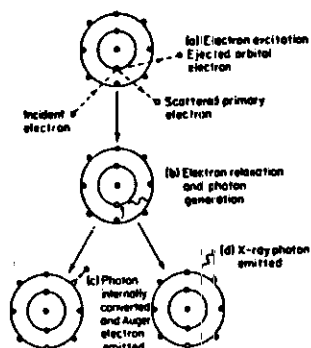


FIG. 10.1 The origin of characteristic x-ray and Auger electrons.

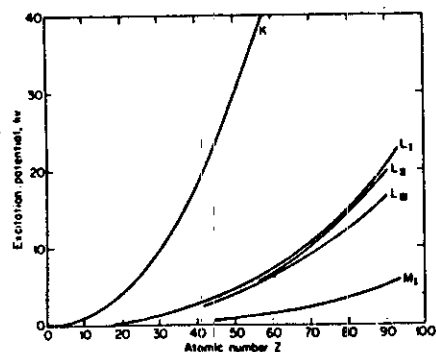


FIG. 10.2 Excitation potential as a function of atomic number.

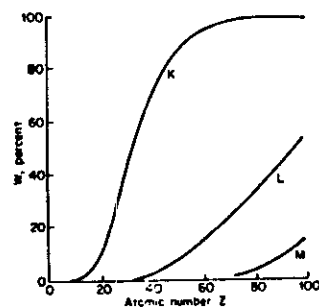
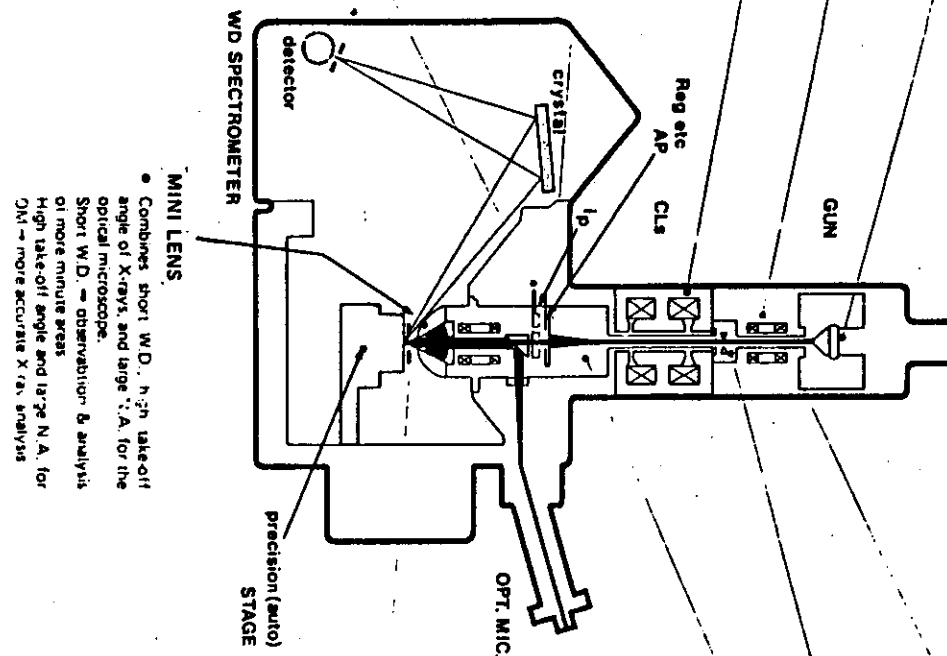


FIG. 10.3 The dependence of fluorescent yield on atomic number Z.



## WDS MICROPROBE ANALYSIS

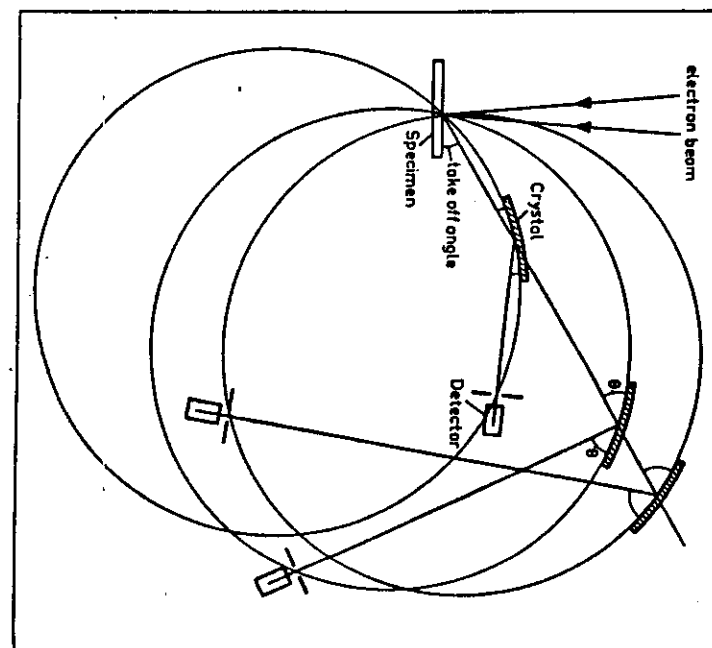
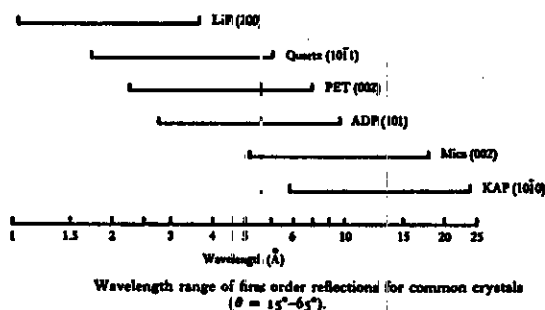
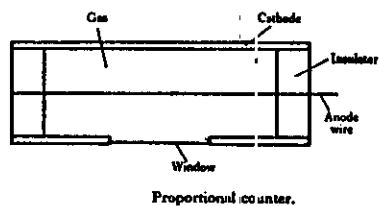
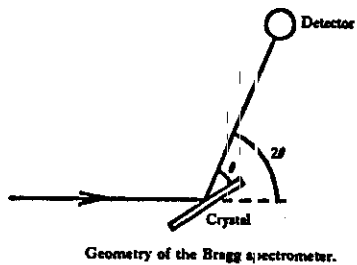


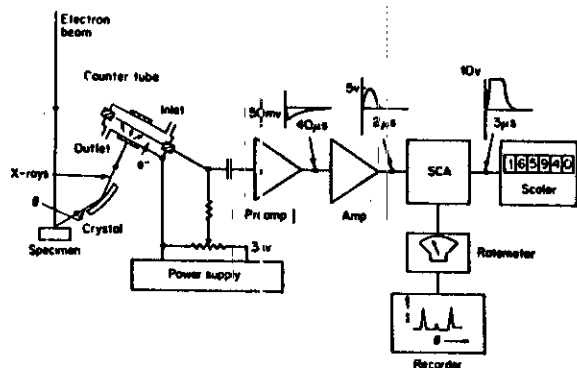
Fig. 1. Basic geometry of crystal spectrometer showing three different positions of the crystal at different Bragg angles.

# X-RAY DIFFRACTION SPECTROMETERS

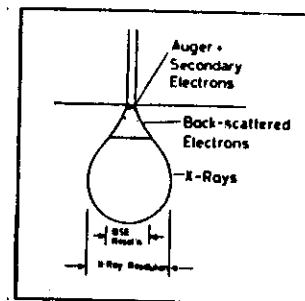
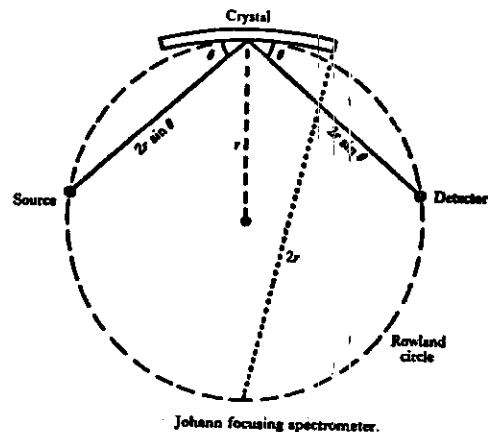
WDS



$$n\lambda_s = 2d \sin \theta_g$$

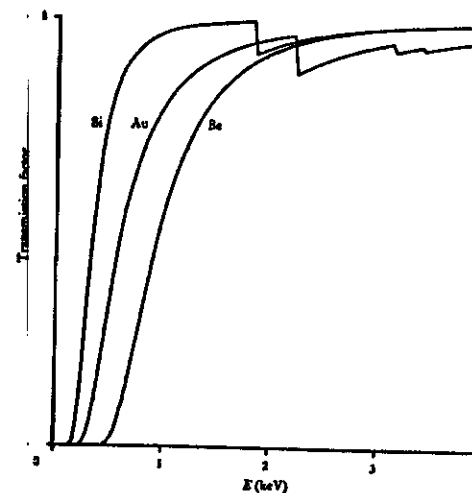
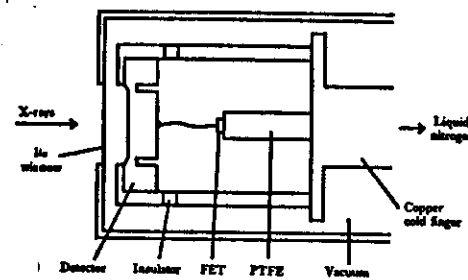


## ELECTRON MICROPROBE ANALYSIS



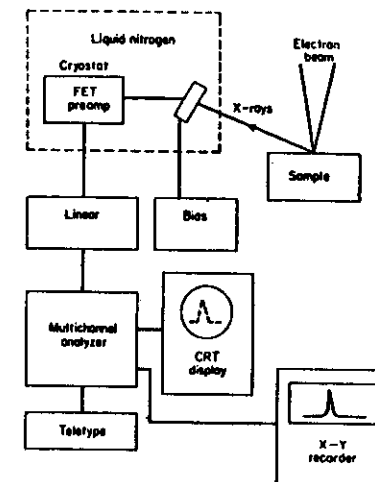
$$d_x = 0.2 - 2 \mu m$$

## LITHIUM DRIFTED SILICON DETECTORS



Transmission of beryllium window (8  $\mu m$ ), gold layer (50 nm), and silicon dead layer (0.1  $\mu m$ ) as a function of X-ray energy (E).

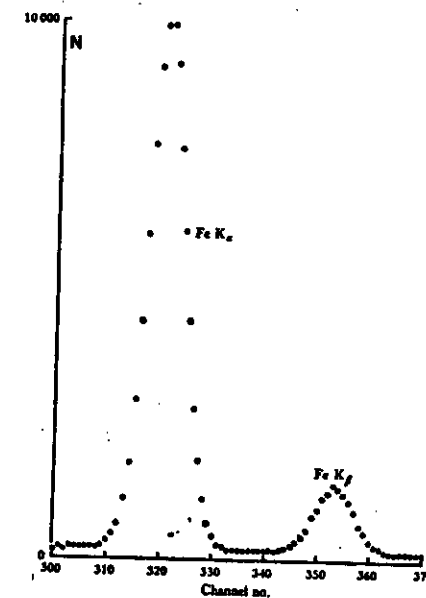
EDS

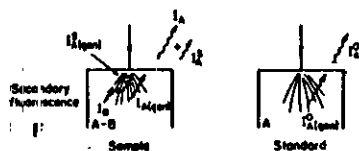
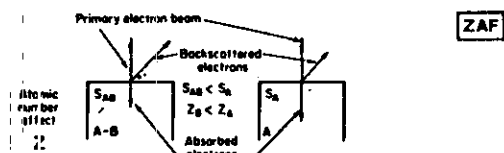


Si(Li) EDS

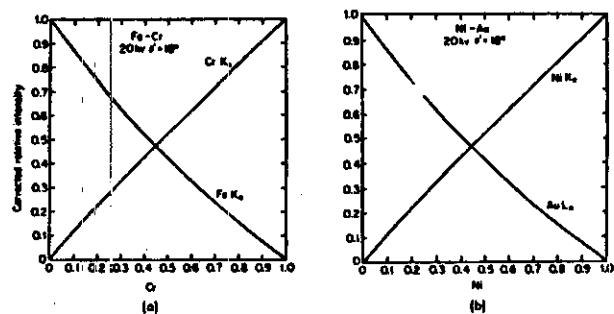
$$\text{charge } n = \frac{E}{3.8 \text{ eV}}$$

FWHM = 140 ~ 180 (220) eV at 5.9 KeV





Schematic illustration of the origin of the ZAF correction factors.



Binary calibration curves: (a) Fe-Cr system; (b) Ni-Au system. Horizontal axis is weight fraction.

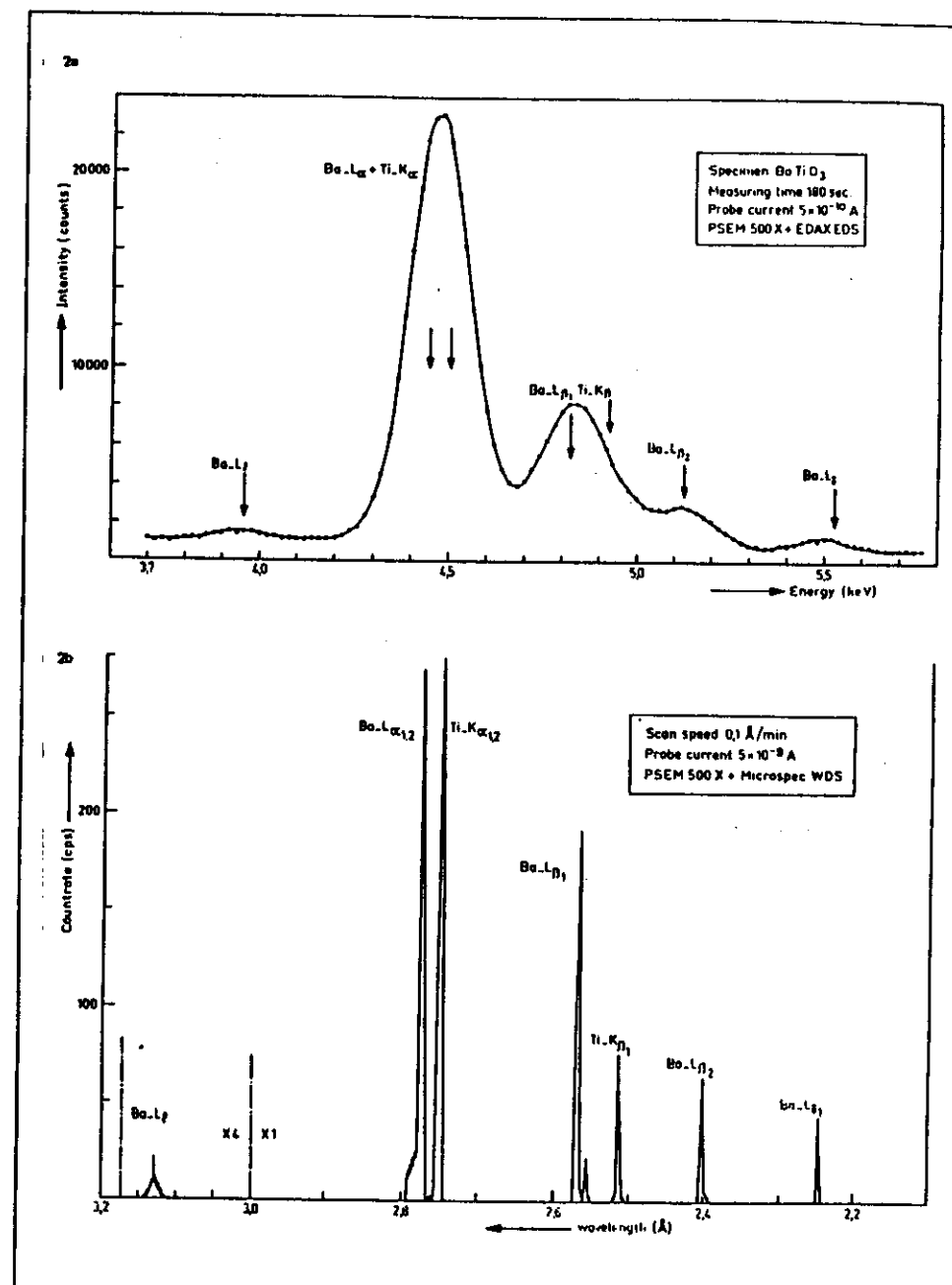
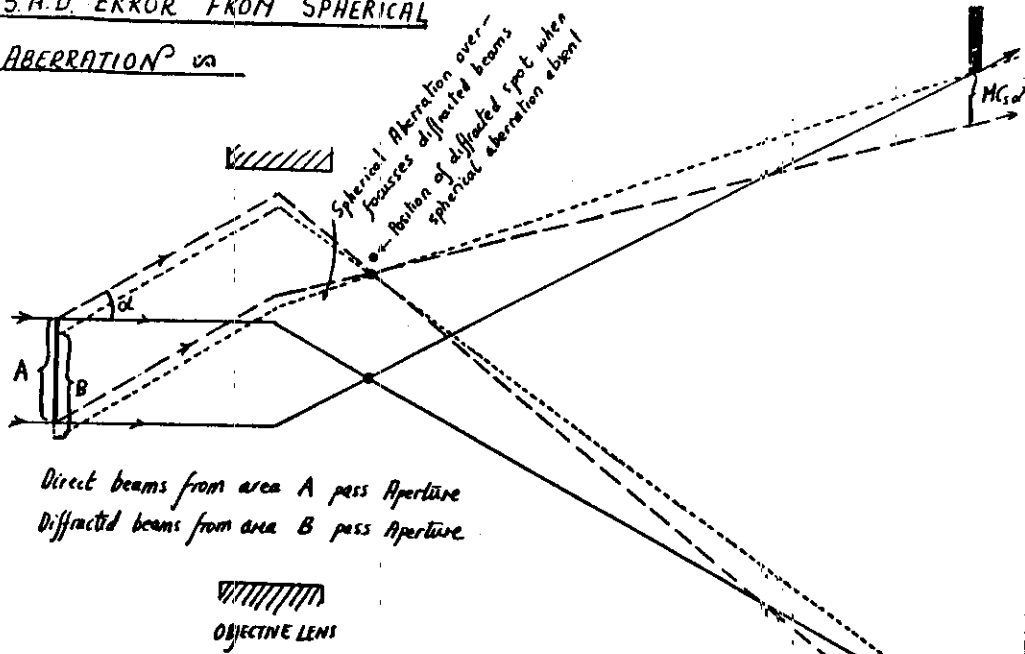


Fig. 2 X-ray spectrum of BaTiO<sub>3</sub>: a) EDS; b) WDS.

## S.A.D. ERROR FROM SPHERICAL

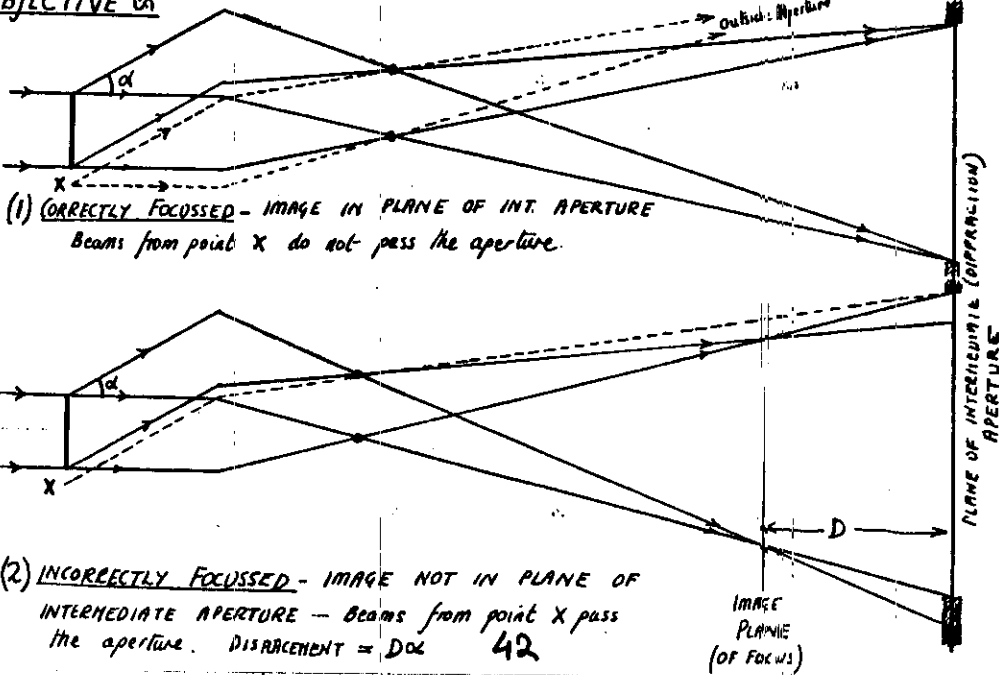
### ABERRATION<sup>2</sup> vs



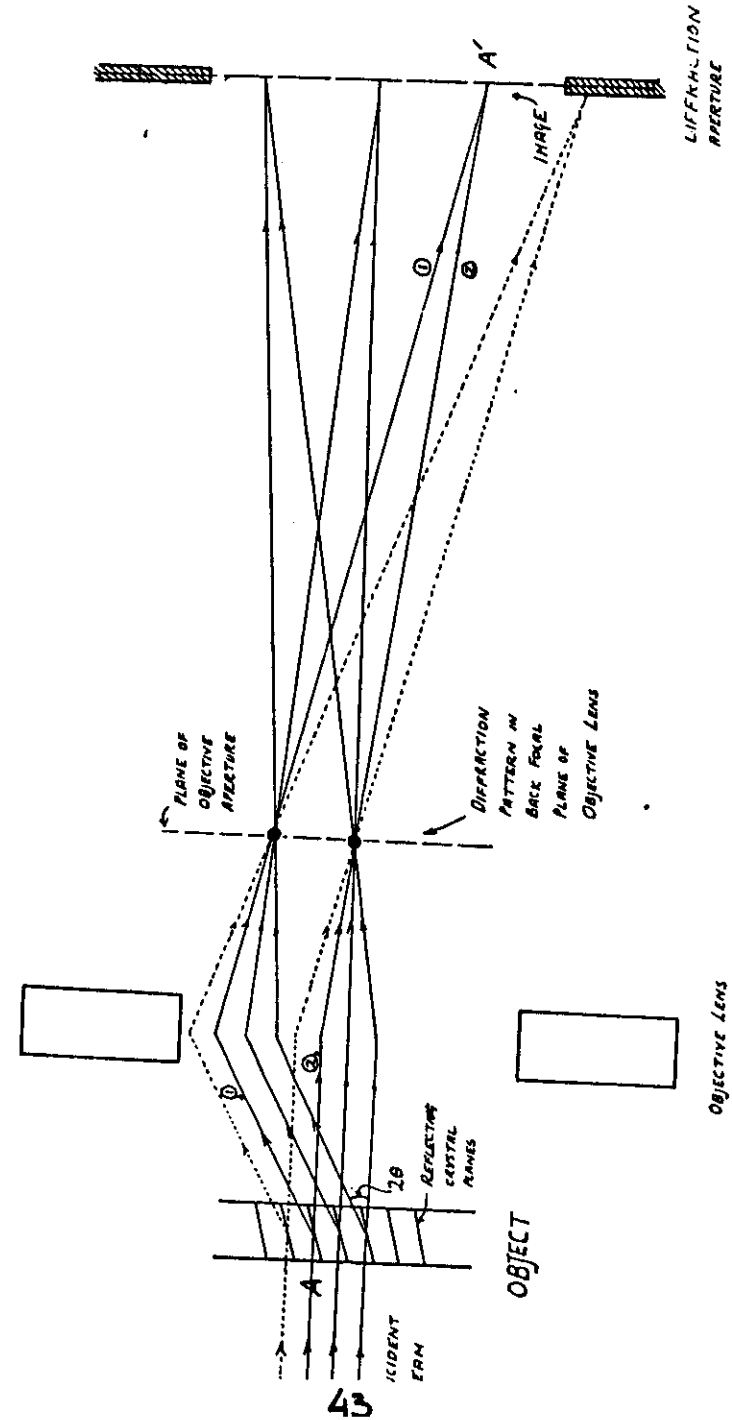
Area B is displaced downwards a distance  $C_s \alpha^3$

## S.A.D. ERROR FROM INCORRECTLY FOCUSED

### OBJECTIVE vs

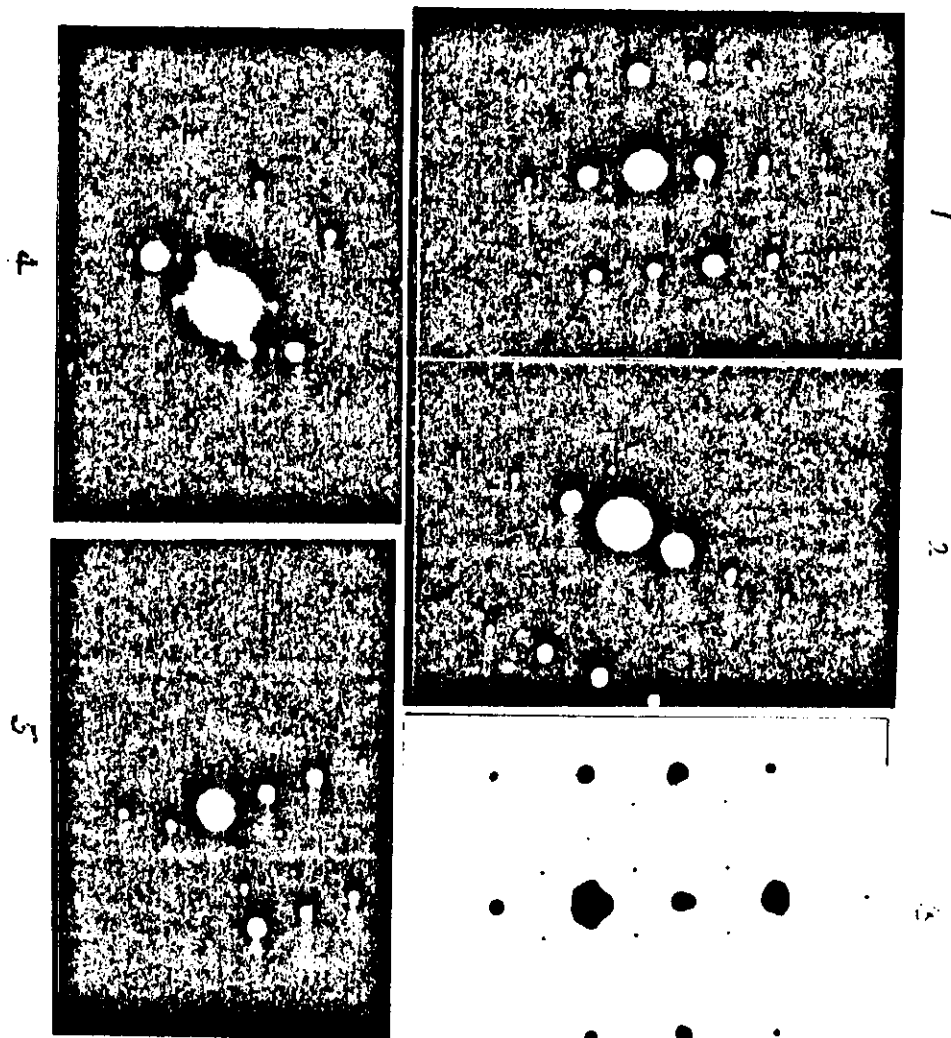


## PRINCIPLES OF IMAGE FORMATION IN THE ELECTRON MICROSCOPE



DIFFRACTION PATTERN EXAMPLES

- (1) Copper specimen  $\lambda L = 8$  mm.  
Index all the spots in the pattern
- (2) Copper specimen  $\lambda L = 8$  mm.  
Index all the spots in the pattern.
- (3)  $\alpha$ -iron specimen containing an f.c.c. precipitate  $\text{Fe}_2\text{TiSi}$ .  $\lambda L = 8$  mm. Index the  $\alpha$ -iron pattern. Index the  $\text{Fe}_2\text{TiSi}$  pattern by inspection and hence determine the orientation relationship between  $\alpha$ -Fe and  $\text{Fe}_2\text{TiSi}$  and the  $\text{Fe}_2\text{TiSi}$  lattice parameter.
- (4)  $\alpha$ -titanium (h.c.p.) specimen showing double diffraction spots, a simple low order zone  $\langle 11\bar{2}0 \rangle$  and several high order zones. Index the reflections in the  $\langle 11\bar{2}0 \rangle$  zone and the high order zone. What is the angle between this zone axis and  $\langle 11\bar{2}0 \rangle$ .
- (5)  $\beta$ -titanium (bcc) containing  $\omega$  precipitates.  
(not included in these exercises).



# BURGERS VECTOR DETERMINATION

Dislocations A to G in the Figure are from different  $111$  type reflections in different  $\langle 211 \rangle$  type zones of copper after tilting the foil.

- In Fig. a)  $g = \bar{1}11$  in  $[211]$  zone  
 b)  $g = 11\bar{1}$  in  $[112]$  zone  
 c)  $g = 1\bar{1}1$  in  $[12\bar{1}]$  zone

From the visibility/invisibility criterion i.e.  $g \cdot b = 0$  when dislocations are invisible, determine whether the dislocations are glissile i.e.  $\frac{a}{2} [110]$ ,  $\frac{a}{2} [101]$  or  $\frac{a}{2} [011]$  or prismatic i.e.  $\frac{a}{2} [110]$ ,  $\frac{a}{2} [101]$  or  $\frac{a}{2} [011]$

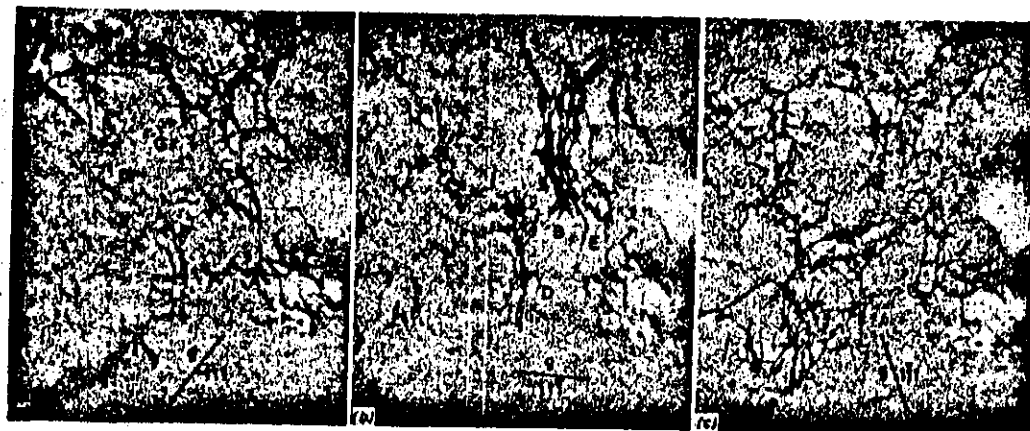
First of all calculate  $g \cdot b$  in the table below for the relevant operating reflections ( $g$ )

b	g · b			
	g	111	11 $\bar{1}$	1 $\bar{1}$ 1
$\frac{a}{2}$ [110]				
$\frac{a}{2}$ [101]				
$\frac{a}{2}$ [011]		1	0	0
$\frac{a}{2}$ [1 $\bar{1}$ 0]				
$\frac{a}{2}$ [10 $\bar{1}$ ]				
$\frac{a}{2}$ [01 $\bar{1}$ ]				

Then by deciding whether the dislocations A to G are visible or invisible under the 3 different operating reflections, deduce from the above table the Burgers vector of each dislocation and therefore decide whether they are glissile or prismatic as shown

below:

Dislocation	[211] [112] [121]			Burgers Vector	Dislocation Type
	$\bar{1}11$	$11\bar{1}$	$1\bar{1}1$		
A	Visible	Invisible	Invisible	$\frac{a}{2} [011]$	Prismatic
B					
C					
D					
E					
F					
G					





Outline a theory for the diffraction contrast produced by a typical defect in a crystalline specimen when studied under two-beam conditions in the transmission electron microscope.

A specimen cut as a (111) section from a deformed sample of a face-centred cubic metal exhibits four separate features with the following characteristics:

(i) when viewed in bright field using an approximate beam direction  $B = [211]$  and strong reflection  $g = \bar{1}\bar{1}\bar{1}$ ,

feature A—a dark line

feature B—a dark line approximately perpendicular to feature A

feature C—a narrow area exhibiting several strong fringes parallel to its long dimension

feature D—a dark line along  $[01\bar{1}]$ ;

(ii) when viewed in bright field with  $B = [112]$  and  $g = \bar{1}\bar{1}\bar{1}$ ,

feature A—invisible

feature B—faint dark line perpendicular to  $[\bar{1}\bar{1}0]$

feature C—a narrow area exhibiting several strong fringes parallel to its long dimension

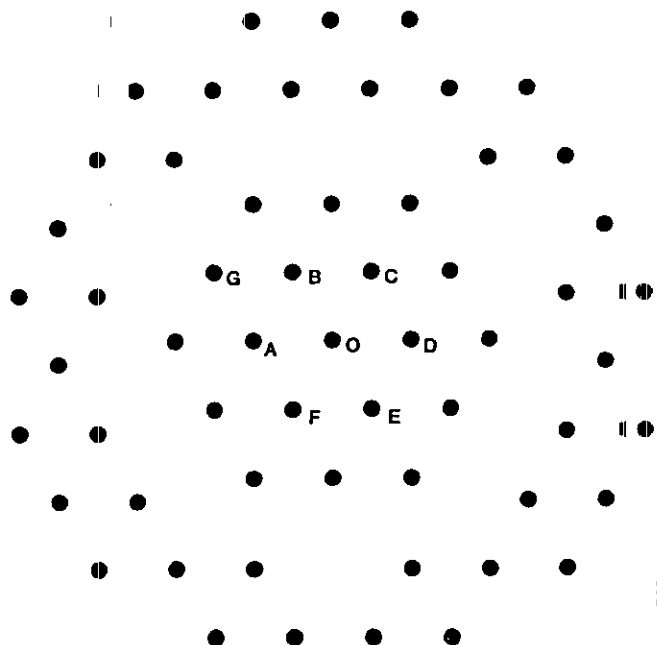
feature D—similar to feature C, but not in the same orientation.

Suggest possible defect configurations which could give rise to these contrast features and describe the additional images you would need to confirm your hypotheses.

2. With the aid of a schematic diagram, describe the principles of construction and operation of a transmission electron microscope. Indicate the positions of planes conjugate to the specimen plane when the microscope is used to form an image, and describe how a diffraction pattern of a small area of the specimen can be recorded.

The figure is a tracing of a diffraction pattern observed from a thin single crystal of aluminium (lattice parameter 400 pm) using electrons with wavelength 4 pm. The spot formed by the undiffracted beam is O. The distances OA, OB and AB are all equal to 1.5 cm. Using the spots lying within a circle of radius 3.5 cm, centred on O, determine the indices of the plane of the crystal normal to the electron beam, give a consistent set of indices to the spots A, B, C, D, E, F and G, and calculate the effective camera length (the effective distance between the specimen and the film on which the pattern was recorded).

Suggest a reason for the presence of the spots lying further than 4 cm away from O.



10. Describe mechanisms by which fast electrons may be inelastically scattered in a crystal.

An electron diffraction pattern of a single crystal consists of discrete Bragg spots together with pairs of Kikuchi lines. Explain how these lines arise and show that the excess line of a pair is further from the direct beam spot.

A thin foil of aluminium with (001) surface is bisected by a small-angle (110) tilt boundary, with tilt axis  $[1\bar{1}0]$  and tilt angle 3 mrad. Two electron diffraction patterns are taken with the electron beam incident normal to the foil, from small areas on opposite sides of the boundary. If the 220 diffraction spot is 50 mm from the centre (000) spot, calculate the displacement of the 220 Kikuchi lines between the two patterns.

(Electron wavelength  $\lambda = 4$  pm; lattice parameter of aluminium  $a = 400$  pm.)

9. Explain how (a) diffraction, (b) spherical aberration and (c) chromatic aberration can limit resolution in microscopy. Discuss the relative importance of the above effects in optical and electron microscopy.

Estimate the size of the smallest feature that can be resolved in a very thin specimen using a 100 kV transmission electron microscope in which the energy spread,  $\Delta E$ , of the electron beam is 1 eV and the chromatic aberration coefficient,  $C_c$ , of the objective lens is 1 mm. How would your answer be affected if a thicker specimen were used, giving rise to an electron energy spread of 20 eV? (You may assume that the resolution of this electron microscope is limited only by diffraction and chromatic aberration, and that for small-angle scattering the radius of the disc of least confusion, referred back to the object plane, due to chromatic aberration is given by  $C_c \alpha \Delta E/E$ , and that due to diffraction is given by  $0.61\lambda/\alpha$ , where  $\alpha$  is the numerical aperture.) Explain how energy spreads in the range 1–20 eV arise.

3. Discuss the origin of 'spot' and 'Kikuchi line' patterns in transmission electron diffraction and show their relationships to each other, to the incident electron beam and to the crystalline specimen producing them.

A parallel beam of electrons of energy 100 keV is incident on a single crystal specimen of aluminium along its  $[110]$  direction. The transmitted electrons are brought to a focus by a set of lenses of effective focal length 1.0 m. Describe as fully as you can the resultant diffraction pattern on a circular screen of diameter 80 mm.

[Aluminium is face-centred cubic, with lattice parameter 405 pm, wavelength of electrons 3.7 pm]

